Quiescent Periods in Helicopter Landing on Ships

Krzysztof Bisewski, Bart M. de Leeuw, Bart Kamphorst,
Hans Kraaijevanger, Ivan Kryven, Julia Kuhn, Alberto Montefusco*,
Michael Muskulus, Tommaso Nesti, Yuliia Orlova, Mark Peletier

Abstract

The problem of helicopter landing on ships has been recently studied by MARIN (MAritime Research Institute Netherlands) with the purpose of helping the naval crew, and in particular the HLO (Helicopter Landing Officer), to take decisions in a fast and reliable way. The basic issue consisted in the prediction of time intervals, called *quiescent periods* (QPs), where the ship motion is sufficiently moderate for the helicopter to be able to land in safe conditions. The ingredients at our disposal were a set of wave data that were simulated by MARIN with their proprietary software FREDYN. Our first goal, then, was to study the statistics of QPs and to identify patterns. The second objective was to use the same data to make predictions on the basis of a few deterministic and stochastic models. The results show that these models are indeed able to capture several features of the waves, such as repetitions of special patterns and memory effects, and surely deserve further investigation and extension. The last approach was purely analytical: after realizing that a sum of one, two and three harmonics already contains sufficient information for the definition of a QP and to get a feeling of the problem, we gave estimates for the frequency and probability of QPs in a signal composed of many random harmonics.

KEYWORDS: helicopter landing on ships, quiescent period, sea waves, narrow-banded signal, random harmonics, level crossing, stationary process, autoregressive model, logistic regression, change-point detection, forecasting, Markov chain

1 Introduction

"–Well, you must understand, signore,
that the scirocco blows for three days if it starts on Tuesday.
Nine days if it starts on Friday.
But if it hasn't blown itself out by the tenth day,
then it goes on for 21 days."

from L. Visconti's screen adaptation of Death in Venice
by THOMAS MANN

*corresponding author

Marine operations, both civilian and military, often require a helicopter to land on a ship or other vessel. Safely landing a helicopter requires the landing pad to be approximately stationary for a period of twenty or thirty seconds. Often, such *quiescent periods* (QP) alternate with periods of stronger ship motion, in which landing is impossible. In such cases a *Helicopter Landing Officer* (HLO) on the ship is responsible for guiding in the helicopter and coordinating its descent.

The landing operation consists of two phases. In the first phase, the HLO assesses the general state of the sea at that moment. This is done on the bridge or inside a cabin, and in this phase the HLO observes the sea and has access to a variety of instruments. When the HLO decides that the frequency of quiescent periods is sufficiently high, he signals the helicopter to approach the ship and to start hovering above the landing pad, and takes position outside, next to the landing pad, in view of the helicopter.

In this second phase the HLO maintains eye contact and radio contact with the helicopter pilot, and observes the ship motion through his legs and eyes. When the HLO believes that a quiescent period is imminent, he signals the pilot to land on the pad. During this operation the pilot has no view of the deck, and is completely dependent on the HLO for guidance.

MARIN (MAritime Research Institute Netherlands) is a Dutch organization with the broad goal of studying operations and decommissioning of ships and offshore platforms, bulk and surface hydrodynamics, as well as nautical training and regulations. Currently, they have an open project on helicopter landing on ships, with which they decided to participate in the SWI 2017. The problem posed by MARIN consists of two questions, each related to one of the two phases described above.

First, MARIN is interested in the distribution of quiescent periods in ship motion, given a certain sea state. This would help the HLO to judge whether the ship motion allows for the helicopter landing to take place in the following minutes with a reasonable accuracy.

Secondly, to make the final phase both more efficient and safe, MARIN would like to give the HLO a further instrument to predict the initiation of quiescent periods with a very short advance, in the order of few seconds. This is why, in our work, we developed tools for predictions, given a history of signals of ship motion.

This report is about the properties of certain *signals*. We will be considering two types of signals:

- *Synthetic* signals, created by adding harmonics (sines and cosines, or complex versions of these) with varying frequencies and amplitudes;
- *Data* signals, given to us by MARIN, which describe the movement of the ship in response to certain "sea states".

In reality MARIN generated the data signals by feeding certain well-chosen synthetic signals as "wave input" to a ship simulator called FREDYN, which outputs the movement of a specific ship in response to these waves. For the purposes of this report, however, we consider these data as "externally given".

The data are time series of the motion of a ship under a predefined wave spectrum. As a ship, for our purposes, may be considered as rigid body, what really matters for us is the set of the six coordinates that fully characterize the motion. In marine jargon, these coordinates assume specific names, which are shown in Table 1.

name	*symbol*	*meaning*
heave	z	vertical motion
sway	y	lateral motion
surge	x	longitudinal motion
pitch	θ	rotation about y-axis
roll	ϕ	rotation about x-axis
yaw	ψ	rotation about z-axis

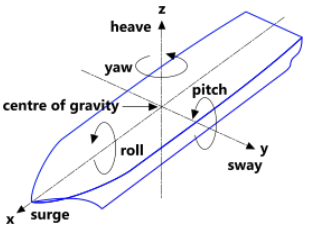

Table 1: Nomenclature for ship motion in marine jargon. CalQlata

In Sec. 3, we will give more details on this set of data: how it has been generated, how we have used it and what we can say about it. Before doing that, in Sec. 2, we will give a short review of the basic theory of signals that is needed in this report, and in Sec. 4 we will study synthetic signals from an analytical viewpoint. In Sec. 5, we will model the data signals by means of various techniques, with the common aim of predicting quiescent periods.

2 Some signal theory

2.1 Signals

For us, signals are functions defined on $\mathbb{R}$ (as for synthetic signals) or on a discrete set (as for the data), with values that are real or complex. Given a signal f on $\mathbb{R}$, the Fourier transform $\mathcal{F}(f)$ or $\hat{f}$ is the complex-valued function of frequency ω given by

$$\hat{f}(\omega) = \frac{1}{\sqrt{2\pi}} \int_{\mathbb{R}} f(t) e^{-i\omega t}\, dt.$$

As it stands, this integral is only defined if $f \in L^1(\mathbb{R})$; however, a natural extension exists Stein and Weiss (1971) to the set of all tempered distributions $\mathcal{S}'(\mathbb{R})$, by exploiting Parseval's theorem

$$\int_{\mathbb{R}} \hat{f}(\omega)\hat{g}(\omega)\, d\omega = \int_{\mathbb{R}} f(t) g(t)\, dt. \tag{1}$$

We will use this extension without mentioning it.

In the discrete case, the signal is only sampled at a finite number of points in time $x_0, x_1, \ldots, x_{n-1}$. Usually these points are multiples of a sampling interval Δ, i.e., the t-th sample x_t is observed at time $t\Delta$. The discrete Fourier transform is then

$$\hat{x}(\nu) = \frac{1}{n} \sum_{t=0}^{n-1} x_t e^{-2\pi i \nu t}. \tag{2}$$

Similar to the continuous Fourier transform, the harmonic functions implicit in Eq. 2 are orthogonal when the frequencies are restricted to the set of *Fourier frequencies*, $\nu_j = j/n$,

$$\sum_{t=0}^{n-1} e^{-2\pi i\nu_j t}\overline{-e^{2\pi i\nu_k t}} = \sum_{t=0}^{n-1} e^{-2\pi i\nu_j t}e^{2\pi i\nu_k t} = \begin{cases} n & \text{if } j \equiv k \pmod n, \\ 0 & \text{otherwise,} \end{cases}$$

and this guarantees the existence of the inverse transform,

$$x_t = \sum_j \hat{x}(\nu_j)e^{2\pi i\nu_j t}. \tag{3}$$

The discretization leads to two phenomena: frequencies higher than the *Nyquist frequency* $1/(2\Delta)$ have an alias in the interval $0 \le \nu \le 1/(2\Delta)$, i.e., appear as an artificial contribution to one of these frequencies. A second undesirable phenomenon is *leakage*, i.e., the appearance of a contribution in the transform at a frequency ν because of the presence of a signal at a different frequency ν_0. This happens (only) if the frequency ν_0 is not a Fourier frequency. More details about this and other practical aspects of Fourier analysis can be found in Bloomfield (2000).

2.2 The harmonics

The *harmonic functions* are an important set of examples. If $f(t) = \cos\omega_0 t$, then $\hat{f}(\omega) = \sqrt{\pi/2}(\delta_{\omega_0} + \delta_{-\omega_0})(\omega)$, where δ_{ω_0} is the Dirac delta function at ω_0; if $f(t) = \sin\omega_0 t$, then $\hat{f}(\omega) = -i\sqrt{\pi/2}(\delta_{\omega_0} - \delta_{-\omega_0})(\omega)$; and if $f(t) = e^{i\omega_0 t}$, then $\hat{f}(\omega) = \sqrt{2\pi}\delta_{\omega_0}(\omega)$. These examples illustrate the general fact that the function f is real-valued if and only if $\hat{f}$ is conjugated-even, i.e. $\hat{f}(\omega) = \overline{\hat{f}(-\omega)}$; similarly, f is purely imaginary iff $\hat{f}$ is conjugated-odd.

Consider the function $f(t) = ae^{i\omega_0 t}$, where $\omega_0 \in \mathbb{R}$ and $a \in \mathbb{C}$. The number ω_0 is called the *angular frequency* and is expressed in radians per second. It can be written as

$$\omega_0 = 2\pi\nu_0, \tag{4}$$

where ν_0 is the *ordinary frequency* expressed in hertz. The word "frequency" can refer to both the angular frequency ω_0 or the ordinary frequency ν_0, depending on the context. The complex number a is called the *complex amplitude*, and contains both the usual amplitude information and information on the phase, since (writing $a = \alpha e^{i\varphi}$, for $\alpha, \varphi \in \mathbb{R}$),

$$ae^{i\omega_0 t} = \alpha e^{i(\omega_0 t+\varphi)} = \alpha\Big[\cos(\omega_0 t + \varphi) + i\sin(\omega_0 t + \varphi)\Big].$$

2.3 Energy spectra and sea states

The *energy spectrum* of a signal f is the real-valued function $\omega \mapsto |\hat{f}(\omega)|^2$. If 'energy' of a function $f \in L^2$ is defined as the L^2-norm $\int |f|^2$, then the value $|\hat{f}(\omega)|^2$ represents

the energy of the Fourier component of f with frequency ω, since from (1) we have

$$\int_{\mathbb{R}} |f(t)|^2 \, dt = \int_{\mathbb{R}} |\hat{f}(\omega)|^2 \, d\omega.$$

An important type of signal is related to the *sea state*, which is a description of the waves at a certain moment. For our purposes, a sea state is defined by an energy spectrum of the waves, as a function of a two-dimensional frequency (ω_1, ω_2), although in the rest of this report we will mostly disregard the two-dimensionality and consider functions of one variable only: the sea state then describes the energy spectrum of a function f of one variable, which describes the waves. In this interpretation f can be interpreted either as giving the wave height at a fixed point in space as a function of time t, or as giving the wave height at a fixed moment in time as a function of a spatial variable x. We will usually consider the former. (Again there is a difficulty here: we want to consider "waves" as elements of $L^\infty(\mathbb{R})$, as in the case of the harmonics, but such waves have infinite spectrum, since $|\delta_\omega|^2$ cannot be defined as a distribution. For these cases the concept of energy spectrum can be made meaningful by considering large intervals and taking a limit under appropriate rescaling. We omit the details.)

The energy spectrum of a function f alone does not uniquely characterize the function f, since it does not contain any phase information. In addition, for simulation purposes the spectrum needs to be discretized. This leads to constructing sample functions f, which are assumed to be representative of the waves, of the form

$$f(t) = \sum_{j=1}^{n} a_j e^{i\omega_j t}, \quad \text{or the real part of this } f,$$

where the a_j and ω_j are chosen randomly from the energy spectrum, in such a way as to make $|\hat{f}|^2$ approximately equal to the assumed spectrum. It is natural in such a setup to choose the distribution of $\arg a_j$, i.e. of the phases, to be uniform on $[0, 2\pi)$, reflecting the fact that the energy spectrum contains no information about the phases.

2.4 Narrow-bandedness and its consequences

We observed that the data provided to us by MARIN is *narrow-banded*: the frequencies present in the signal are concentrated in a fairly narrow interval (see Figure 1). This results in a signal with a fairly recognizable period, and an amplitude that varies on a larger scale.

Because of this narrow-bandedness the time course resembles an amplitude modulation of a fixed-frequency oscillation, and in the rest of this report we use this way of viewing the signals. This has a number of consequences:

1. The essential information in the data is already encoded in the local maxima and minima; in the data processing that we do, we thus first extract the local maxima and minima, and use the sequence of those data points.

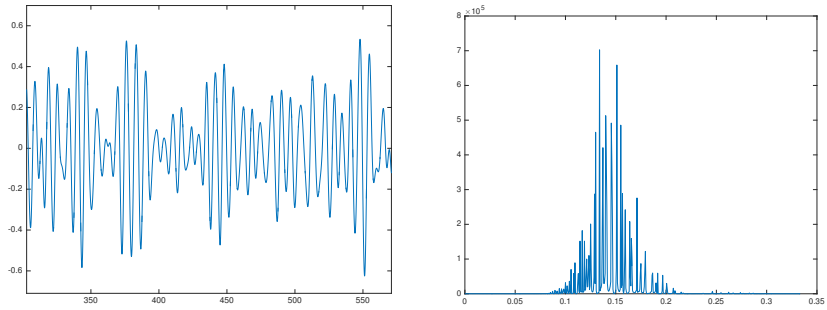

Figure 1: A representative section from *heave* data from MARIN (see the next Section for details). Left is the signal as function of time, right is the spectrum.

2. For the analysis, one would like to concentrate on the properties of the "envelope" that appears "obvious" to the human eye, since quiescent periods of more than a fraction of the period of the underlying oscillation are one-to-one related to periods in which this envelope is small.

We now explore this second aspect more in detail. A real-valued signal has a spectrum that is symmetric with respect to frequency 0; "narrow-banded" for a real-valued signal means that the spectrum is concentrated around ω_0 and $-\omega_0$ for some $\omega_0 \neq 0$.

From any complex signal $f(t)$ one can easily construct a real-valued signal $S(t)$ by taking its real part,

$$S(t) = \operatorname{Re} f(t). \tag{5}$$

The inverse operation is not unique, however, since there obviously exist many complex-valued signals with the same real part. We can use this freedom of constructing a well-chosen complex counterpart of a given real-valued signal to make the spectrum appear only at positive frequencies. Given a real-valued signal S, its associated *analytic signal* f is defined by concentrating all of the Fourier transform on the *positive* frequencies, i.e. we set

$$\hat{f}(\omega) := \begin{cases} 0 & \omega < 0 \\ \hat{S}(0) & \omega = 0 \\ 2\hat{S}(\omega) & \omega > 0. \end{cases}$$

After transforming $\hat{f}$ back to f, the function f is now complex-valued, and can be interpreted as a an "interpolated" version of the function S, in the sense that (5) holds; and it is an interpolated version that "only rotates in one direction" in the complex plane, as shown in Figure **??** The function f can also be represented as

$$f(t) = S(t) + iHS(t), \tag{6}$$

where HS is the Hilbert transform of S.

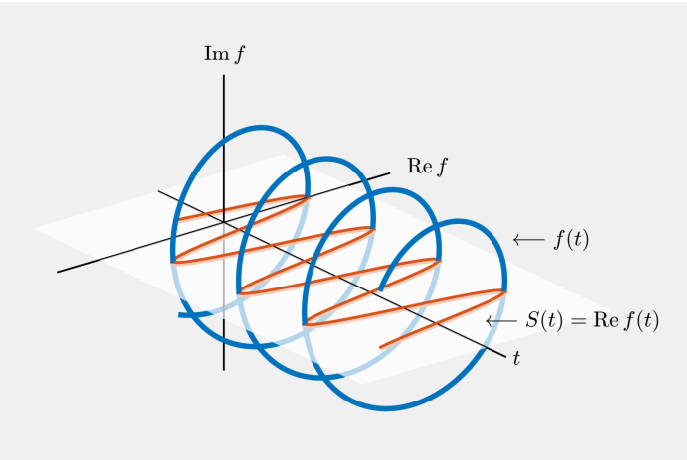

Figure 2: Graphical representation of the *analytic signal*: the red curve is the real signal and the blue complex curve is the corresponding analytic signal, constructed according to Eq. (6).

The analytic signal now gives us an opportunity to make the concept of "envelope" precise. In general, from each complex-valued function $t \mapsto f(t)$ one can define the real-valued *instantaneous amplitude* and *instantaneous phase* by writing

$$f(t) = A(t)e^{i\phi(t)}, \qquad \text{for some } A(t), \phi(t) \in \mathbb{R}. \tag{7}$$

If the function f is continuous, then A and ϕ can also be taken continuous, and A and ϕ are unique up to adding multiples of 2π to the phase.

The property that f is narrow-banded corresponds to the fact that $\phi'(t)$ is close to ω_0. If f is narrow-banded, then A varies slowly (we illustrate this in Section 4.2), and as a result we can use the function A as a working concept for the intuitive idea of the "envelope".

3 Data signals and their quiescent periods

In the last decades several programs have been developed to study the motion of ships under the forcing of sea waves. MARIN uses its own software, denominated FREDYN, which studies the dynamic behavior of a steered ship subjected to waves and wind. A description can be found in the website MARIN. As the software is a proprietary one, MARIN provided us with several sets of data, varying for time length, direction and spectrum of the waves.

The input of the program was a train of waves given by randomly sampling a well-defined spectrum, typical of the North Sea. The output that was relevant for us

consisted of six time series of the six coordinates of ship motion, sampled at regular time intervals.

In our analyses, we mostly focused on the *heave* coordinate *at the landing pad*, since – together with the roll – it is the most important variable for helicopter landing. Although operative conditions for helicopter landing on ships are not well defined by any regulation, there exist such rules for landing on offshore platforms. According to the latter, MARIN suggested the following requirements for a quiescent period:

- peak-to-trough amplitude of *heave* $< 3\,\mathrm{m}$;
- single *roll* amplitude $< 3°$;
- time duration of at least 30 s.

These represent rather strict requirements, which might be relaxed, and are surely too stringent for navy operations.

The first question that MARIN asked us concerns the distribution of quiescent periods. In the present section, we will address this problem by looking at the data signals that we received from MARIN. Some of the data sets were not representative enough either in time duration, or wave spectra didn't include non-quiescent periods. Thus, we considered only a few representative data sets, collected in Table 2.

Alias	U	μ	H_s	T_p	T	Motion sensor
D1	10 kn	180°	3 m	8 s	18000 s	HELI
D2	10 kn	180°	3 m	8 s	7200 s	HELI
D3	10 kn	180°	3 m	8 s	1800 s	HELI (wave spreading)
D4	10 kn	180°	5 m	8 s	1800 s	HELI

Table 2: Data sets generated by the computer program FREDYN. The meaning of the simulation parameters is as follows: U - ship speed, μ - wave direction, H_s - significant wave height, T_p - peak wave period, T - simulation time.

3.1 Distribution of Quiescent Periods

In this section, we will describe the procedure of data pre-processing and the idea of finding QPs in the considered system. According to MARIN's definition of QPs explained above, only several data sets were suitable for this analysis as for some data sets the system never went out of the quiescent state.

First of all, roll and heave are chosen as the most representative coordinates. Due to the definition of the QPs, only extrema of the signals of these two coordinates are taken into account as points lying between extrema don't contribute to the analysis. For purposes of convenience, we suggest to work with absolute values of signals. In this case, the *single amplitude* is the height of the peak; the *peak-to-trough amplitude* is the sum of heights of two neighboring peaks.

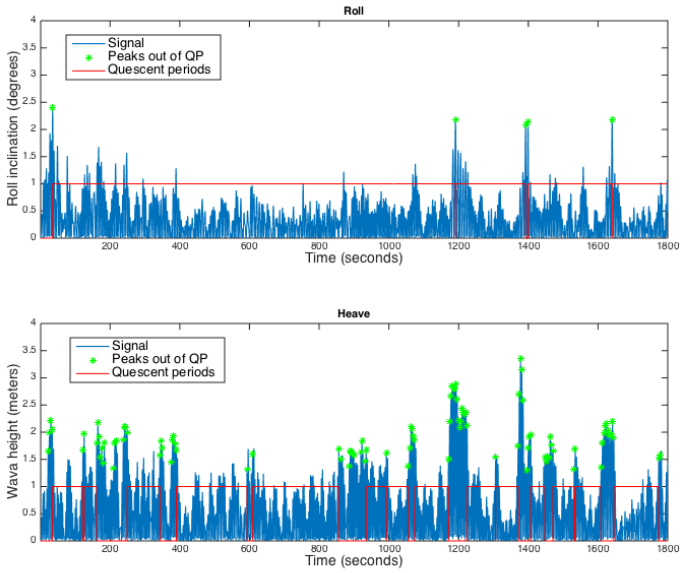

Figure 3: Example of quiescent periods found in a raw data for roll and heave signals

In Figure 3 one can see the absolute values of signals for roll and heave coordinates from data D4 from Table 2. It appeared that in all data sets the signal for the roll coordinate was not exceeding the threshold of 3°. Thus we agreed with MARIN to lower the threshold for single roll amplitude from 3° to 2° in order to illustrate the whole QP search procedure. Green asterisks denote those peaks that do not fall into the definition of the QP for the considered coordinate. Thus, the QPs are those areas, which lie between green asterisks. In the plot we illustrate QPs with an indicator function, which takes the value 1 if extrema are in a QP, and 0 otherwise:

$$\mathbb{1}_{QP} = \begin{cases} 1, & x \in \text{QP} \\ 0, & \text{otherwise.} \end{cases}$$

As we have separate QPs for roll and heave, we can determine QPs for the whole system. For this purpose, we take an intersection of these areas for both signals. According to the definition, we consider only those periods that last longer than 30 seconds.

Further, we would like to look at the distribution of the duration of QPs. From Figure 3 we can see that the statistics of QPs is not good enough. Thus, we apply the same search procedure on the data set from the longer simulation of 18000 seconds

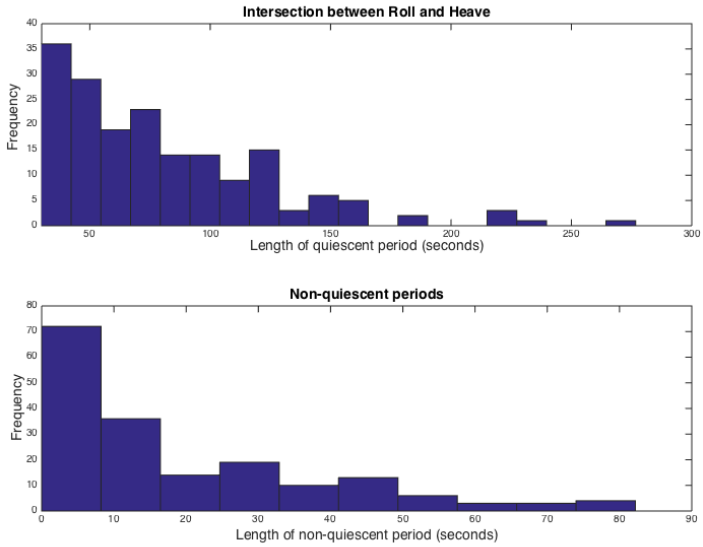

Figure 4: Distribution of the duration of quiescent (up) and non-quiescent (down) periods in a data set of 18000 s

(D1). On the upper plot in Figure 4 we can see how often QPs with different duration appear in the system. The lower plot in Figure 4 corresponds to the distribution of the time intervals when the system is not in a QP.

From the plot in Figure 4 we notice that the distribution of the time intervals for QPs reminds of the shape of the probability density function of the exponential distribution, which is the case to model the occurrences of random events as Poisson process. This observation may be verified by statistical hypothesis testing, which has not been done in the current work. Furthermore, the histogram of the durations of QPs captures the information about the sea state in a specific time interval. Thus, it could help HLO to judge the behavior of the sea and estimate how many QPs one might expect in the current situation.

3.1.1 Summary

The aim of this section was to e the data signals generated by FREDYN and gain an idea about the nature of the occurrences of QPs in waves. Upon analyzing the histogram of the durations of QPs, one may assume that the data follows an exponential distribution. However, to conclude this, we would need to analyze longer simulations with more variations in the wave profile and perform a statistical hypothesis test. If the test confirms the exponential distribution, one might consider to model the occurrences of QPs according to a Poisson process.

3.2 Qualitative patterns

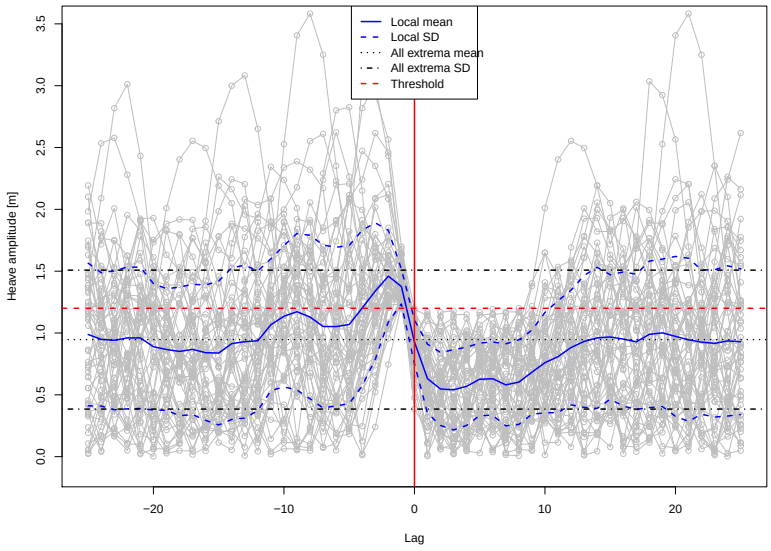

Figure 5: Transition to quiescent period in the data set D2. Shown are subsequent absolute values of extrema of the heave signal, conditional on the event that a quiescent period starts (marked by red vertical line). For simplicity, here the quiescent period has been defined to be at least 30 seconds of heave signal below a threshold value of 1.2 m. The mean and standard deviation of the individual time traces are indicated (blue curves), as well as the overall mean and standard deviation of the (absolute values of) extrema (black lines).

An interesting way of studying qualitative patterns in the signal related to QPs is the use of *event-related analysis*. After QPs have been defined and identified in the signal, one cuts the time series into short segments around the beginning of each QP and aligns these periods such that the QPs start at the same relative time (or lag). An example is shown in Figure 5 for the extrema of the heave signal in the data set D2. In fact, only the absolute values of the extrema were used in this analysis, as otherwise QPs starting with negative or with positive extrema would be mixed and the relevant information would be averaged out. The start of the QP, i.e., the event used for the alignment of the signals, is marked with a vertical red line. The condition imposed by the event is that the first extremum before the event has to lie above the threshold (marked by the horizontal red line), and the first extremum inside the event has to lie below it.

What is somewhat unexpected, and therefore interesting, is that the extrema seem to have been higher than average already for about 5 waves (equal to 10 extrema) before the event, on average. The length of this period corresponds to the average length of the QP in this case, which is also about 5 waves – although this might be a coincidence. After the QP, the statistical properties of the extrema quickly approach the overall distribution indicated in the figure (i.e., the blue curves approach the black lines), within about 4 extrema.

This and related figures (e.g. for different conditions imposed on the extrema) can provide important hints for what patterns are present in the signals and how to exploit these. One example of a more quantitative analysis of these patterns will be given in Sec. 5.4.2.

4 Distribution of QPs by analytic estimates

The motion of the ship is the net result of the mechanics of the ship and the forces exerted on the ship by the waves. Exactly characterizing the forces on the ship that result from the waves is non-trivial, and beyond our scope. Instead of focusing on the ship, we have therefore focused on the waves.

More precisely, we have addressed the question

> Given a signal on $\mathbb{R}$ with specified spectrum and random amplitudes and phases, what is the distribution of quiescent periods?

Again, this requires specification, since a typical spectrum has a full support. Instead we consider signals with discretized spectra, of the form

$$f(t) = \sum_{j=1}^{n} a_j e^{i\omega_j t}, \tag{8}$$

for some finite n, where a_j are complex amplitudes chosen such that the spectrum of f resembles a given spectrum, and such that the phases are uncorrelated. As discussed in Section 2.4 this complex signal f can be 1-to-1 related to a real signal S, which is simply obtained from f by taking its real part (see (5)),

$$S(t) = \sum_{j=1}^{n} \alpha_j \cos(\omega_j t + \phi_j), \tag{9}$$

where $\alpha_j = |a_j|$ and $\phi_j = \arg a_j$. We emphasize that for any real-valued signal S of the form (9) its associated complex signal f is uniquely defined and should be seen as its analytic representation (see Section 2.4).

In the software FREDYN the ship model is driven by one or more of such signals, representing wave trains from different directions. In this case $n \approx 100$, but we will also address the small-n case; it turns out that interesting insight can be gained from $n = 2$ and $n = 3$, for instance.

4.1 Definition of quiescent periods

In the context of a general signal of the form (8), describing the behaviour of waves, it does not make much sense to consider a quiescent period as defined by an absolute criterion. Instead we consider quiescent periods as defined by a relative criterion, characterized by two parameters and a choice of norm:

Definition 4.1. Let $\tau > 0$ and $\theta > 0$ be given. Given a signal of the form (8) a quiescent period is defined by the property

$$\|f\|_{[t,t+\tau]} \leq \theta \,\text{'average'}\big(\|f\|_{[t',t'+\tau]}\big). \tag{10}$$

Here $\|f\|_{[t,t+\tau]}$ can be any norm of f that is calculated over the time section $[t, t+\tau]$; we will consider two different norms below. The parameter θ is a threshold: a quiescent period is a period in which the norm of f over that period is less than θ times the average value of the norm. The 'average' can be interpreted in two ways – either the average over times t', or the expectation over the randomness of coefficients. We will use both below.

4.2 The narrow bandwidth assumption

It is unclear to us how to characterize the rate of occurrence of quiescent periods in a completely arbitrary signal. In order to make the question more amenable to analysis we concentrate in all of Section 4 on the case of *narrow bandwidth*, as discussed in Section 2.4: we assume that there exists a *reference frequency* $\omega > 0$ and a *bandwidth* $\varepsilon \geq 0$ such that

$$|\omega_j - \omega| \leq \varepsilon \ll \omega \quad \text{for all } j = 1, 2, \ldots, n. \tag{11}$$

We refer to Figure 6 for a graphical illustration of this assumption.

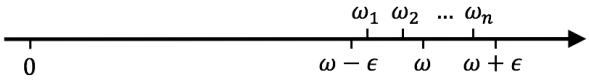

Figure 6: All angular frequencies ω_j are ε-close to the reference frequency ω.

Using the narrow-bandedness assumption, we rewrite the complex signal $f(t)$ defined in (8) as

$$f(t) = e^{i\omega t} f_0(t) \tag{12}$$

so that the function f_0 can be written in terms of the real-valued amplitudes $\alpha_j > 0$ and phases ϕ_j as

$$f_0(t) = \sum_{j=1}^{n} \alpha_j e^{i[(\omega_j - \omega)t + \phi_j]}. \tag{13}$$

Since $f_0(t)$ only differs by a factor $e^{i\omega t}$ from $f(t)$, its polar form

$$f_0(t) = A(t) e^{i\phi_0(t)} \tag{14}$$

has the same instantaneous amplitude $A(t)$ as $f(t)$, whereas the instantaneous phases $\phi(t)$ and $\phi_0(t)$ are related by

$$\phi(t) = \omega t + \phi_0(t). \tag{15}$$

This implies that the corresponding real signal $S(t) = \operatorname{Re} f(t)$ can be written as

$$S(t) = A(t)\cos\phi(t) = A(t)\cos(\omega t + \phi_0(t)). \tag{16}$$

If the bandwidth ε is small, the value $f_0(t)$ moves slowly through the complex plane since it follows from (11) and (13) that its velocity is bounded by

$$|f_0'(t)| \leq \varepsilon \sum_{j=1}^{n} \alpha_j. \tag{17}$$

This not only implies that the instantaneous amplitude $A(t) = |f_0(t)|$ is slowly changing,

$$|A'(t)| \leq |f_0'(t)| \leq \varepsilon \sum_{j=1}^{n} \alpha_j, \tag{18}$$

but also that the angular velocity $\phi_0'(t)$ of $f_0(t)$ is small,

$$|\phi_0'(t)| \leq \frac{|f_0'(t)|}{|f_0(t)|} \leq \varepsilon \frac{\sum_{j=1}^{n} \alpha_j}{A(t)}, \tag{19}$$

provided $f_0(t)$ stays away from the origin. In that case it follows from (15) that the angular velocity $\phi'(t)$ of $f(t)$ is approximately equal to the reference frequency ω,

$$\phi'(t) = \omega + \phi_0'(t) \approx \omega. \tag{20}$$

We conclude that the real signal $S(t) = \operatorname{Re} f(t)$ can be written in the form (16), where the instantaneous amplitude $A(t)$ is the modulus of the slowly varying complex-valued function $f_0(t)$ defined in (13), and the instantaneous (angular) frequency $\omega(t) = \phi'(t)$ is approximately equal to the reference frequency ω (see (20)).

This remark allows us to refocus our attention. The *reference time period* associated with the reference frequency ω is given by

$$T = \frac{2\pi}{\omega}. \tag{21}$$

In practice, the minimal length τ of a quiescent period is significantly longer than T. This implies that the real-valued signal S can only be small over a time τ if the amplitude A also is small over that period (i.e., the smallness can not come from the cosine in (16); it has to come from A). Therefore, in our quest for suitable quiescent periods we can limit ourselves to time intervals where the instantaneous amplitude $A(t)$ is small; or equivalently, we can focus on f_0 instead of f. Our aim therefore becomes

> Find periods (or characterize the probability of periods) such that the modulated signal f_0 is small over a period τ.

In the following we will first take a "deterministic" approach, which is followed by a "stochastic" approach. In the "deterministic" approach, we derive criteria for the existence of quiescent periods for arbitrary real signals S of the form (9) (and their complex counterpart f defined in (8)). In dedicated subsections we first consider the cases $n = 1$, $n = 2$ and $n = 3$ in detail before we analyze the case of arbitrary n. After completing the "deterministic" case we turn our attention to the stochastic case, where the complex amplitudes a_j of the complex signal f in (8) are stochastic variables. In that case we will study quiescent periods of randomly sampled signals.

4.3 The deterministic case for $n = 1$

If $n = 1$, the real signal $S(t)$ defined in (9) consists of a single cosine,

$$S(t) = \alpha_1 \cos(\omega_1 t + \phi_1), \qquad \alpha_1 > 0,\ \phi_1 \in \mathbb{R}. \tag{22}$$

In this case the bandwidth is equal to $\varepsilon = 0$ and the reference frequency is equal to $\omega = \omega_1$. Quiescent periods longer than the reference value T defined in (21) only occur if α_1 is small enough, and in that case the quiescent period lasts forever.

For completeness we note that the associated complex signal $f(t)$ defined in (8) has instantaneous amplitude $A(t) \equiv \alpha_1$ and instantaneous phase $\phi(t) \equiv \omega_1 t + \phi_1$, showing that $f(t)$ moves on a circle with radius α_1 centered around the origin with uniform angular velocity ω_1. In contrast, the complex signal $f_0(t)$ defined in (13) is constant, and corresponds to a fixed point in the complex plane. In Figure 7 we have displayed the signal $S(t)$ and the (constant) instantaneous amplitude $A(t)$ of its associated complex signal for $n = 1$, $\alpha_1 = 1$, $\omega_1 = 1$, $\phi_1 = 1$.

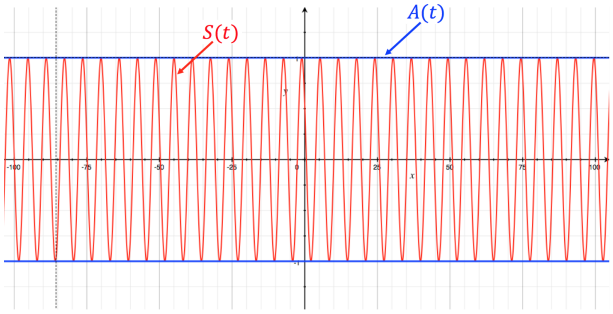

Figure 7: For $n = 1$, $\alpha_1 = 1$, $\omega_1 = 1$, $\phi_1 = 1$ we have displayed the real signal $S(t)$ and the instantaneous amplitude $A(t)$ of its associated complex signal for $t \in [-100, 100]$.

4.4 The deterministic case for $n = 2$

If $n = 2$ we assume without loss of generality that $\omega_1 < \omega_2$. We set $\omega = \omega_1$ so that the bandwidth equals $\varepsilon = \omega_2 - \omega_1$. The complex signal $f_0(t)$ defined in (13) is given by

$$f_0(t) = \alpha_1 e^{i\phi_1} + \alpha_2 e^{i(\varepsilon t + \phi_2)}, \qquad \alpha_1, \alpha_2 > 0,\ \phi_1, \phi_2 \in \mathbb{R}. \tag{23}$$

Clearly $f_0(t)$ moves on a circle with center at $\alpha_1 e^{i\phi_1}$ and radius α_2 with a relatively low constant velocity given by

$$|f_0'(t)| = \alpha_2 \varepsilon. \tag{24}$$

For the corresponding instantaneous amplitude $A(t) = |f_0(t)|$ we find

$$\begin{aligned} A(t) &= |\alpha_1 e^{i\phi_1} + \alpha_2 e^{i(\varepsilon t + \phi_2)}| = |\alpha_1 + \alpha_2 e^{i(\varepsilon t + \Delta\phi)}| \\ &= \sqrt{\alpha_1^2 + \alpha_2^2 + 2\alpha_1\alpha_2 \cos(\varepsilon t + \Delta\phi)}, \end{aligned}$$

where

$$\Delta\phi = \phi_2 - \phi_1.$$

Clearly, A is a periodic function (with period $2\pi\varepsilon^{-1}$) that varies between its minimum $|\alpha_1 - \alpha_2|$ and its maximum $\alpha_1 + \alpha_2$. Quiescent periods only occur if this minimum is small enough. This is the case if α_1 is sufficiently close to α_2. In Figure 8 we have displayed such an example with $\alpha_1 \approx \alpha_2$, $\varepsilon = 0.11$ and $\Delta\phi = -1$.

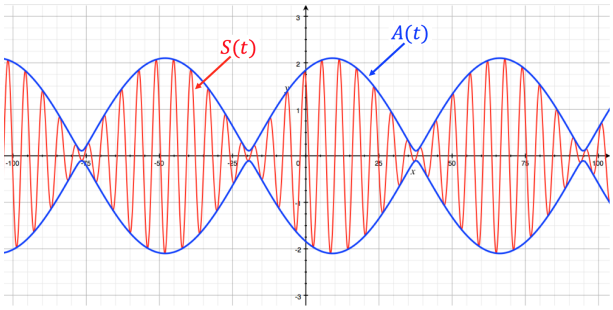

Figure 8: A typical example of a real signal $S(t)$ and the instantaneous amplitude $A(t)$ of its associated complex signal for $t \in [-100, 100]$. Here we have chosen $n = 2$, $\alpha_1 = 1$, $\alpha_2 = 1.1$, $\omega_1 = 1$, $\omega_2 = 1.11$, $\phi_1 = 1$, $\phi_2 = 0$.

4.5 The deterministic case for $n = 3$

If $n = 3$ we assume without loss of generality that $\omega_1 < \omega_2 < \omega_3$. We define $\varepsilon_1 = \omega_2 - \omega_1$ and $\varepsilon_3 = \omega_3 - \omega_2$ (see Figure 9).
Setting $\omega = \omega_2$ the complex signal $f_0(t)$ defined in (13) is given by

$$f_0(t) = \alpha_1 e^{i(-\varepsilon_1 t + \phi_1)} + \alpha_2 e^{i\phi_2} + \alpha_3 e^{i(\varepsilon_3 t + \phi_3)}, \qquad \alpha_1, \alpha_2, \alpha_3 > 0,\ \phi_1, \phi_2, \phi_3 \in \mathbb{R}. \tag{25}$$

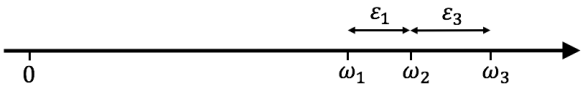

Figure 9: For $j = 1, 3$ the distance $|\omega_j - \omega_2|$ is denoted by ε_j.

This shows that the trajectory of $f_0(t)$ is the result of the superposition of two circular motions with relatively low angular velocities ($-\varepsilon_1$ and ε_3). In Figure 10 we have displayed two such trajectories.

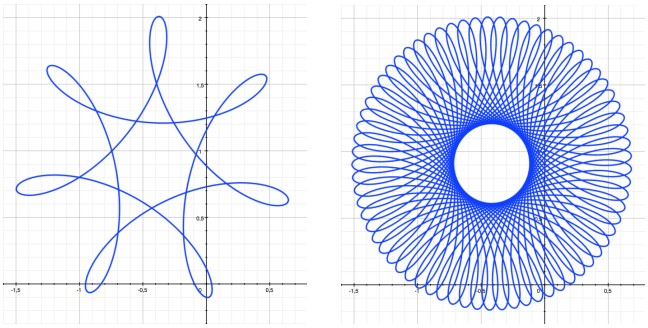

Figure 10: The trajectory of the complex signal $f_0(t)$. In the left figure we have chosen $n = 3$, $\alpha_1 = 0.4$, $\alpha_2 = 1$, $\alpha_3 = 0.7$, $\omega_1 = 0.95$, $\omega_2 = 1$, $\omega_3 = 1.02$, $\phi_1 = 1$, $\phi_2 = 2$, $\phi_3 = 3$. In the right figure we have only slightly changed ω_1 from 0.95 into 0.951.

In general we can distinguish the following two cases:

- **The "rational" case:** the ratio $\varepsilon_3/\varepsilon_1$ is a rational number
- **The "irrational" case:** the ratio $\varepsilon_3/\varepsilon_1$ is irrational

Both cases displayed in Figure 10 are 'rational' since the ratios $\varepsilon_3/\varepsilon_1$ are $2/5$ and $20/49$, respectively. In the general 'rational' case there exist two positive integers k and ℓ such that

$$\frac{\varepsilon_3}{\varepsilon_1} = \frac{\ell}{k}, \tag{26}$$

where we may assume, without loss of generality, that k and ℓ are relatively prime. One easily verifies that in this case the complex signal $f_0(t)$ has a periodic orbit with period

$$\Delta t = 2\pi k \varepsilon_1^{-1} = 2\pi \ell \varepsilon_3^{-1}. \tag{27}$$

For the two cases displayed in Figure 10 the periods are $\Delta t = 200\pi$ and $\Delta t = 2000\pi$, respectively. For the graphs of the corresponding real signals $S(t)$ we refer to Figures 11 and 12. In Figure 11 (which corresponds to the left trajectory in Figure 10) we

see that the amplitude $A(t)$ has indeed a period $\Delta t = 200\pi$ and that each period has exactly one quiescent period. In Figure 12 (which corresponds to the right trajectory in Figure 10) we have limited the time window to $[-300, 2700]$, which is less than half the period $\Delta t = 2000\pi$ of the amplitude $A(t)$. Comparing the latter figure to Figure 11, we see that both graphs are very similar for times in the interval $[-300, 500]$, including the two quiescent periods marked with a black arrow. This is not surprising since the only difference between both cases is a slightly different value of ω_1. For later times, the difference between both graphs becomes more pronounced, which also illustrates the fact that the period of the amplitude $A(t)$ in the second graph is 10 times as large as the amplitude of $A(t)$ in the first graph.

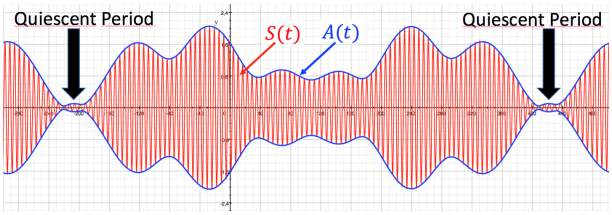

Figure 11: For the case displayed in Figure 10 on the left, this is the graph of the real signal $S(t)$ (in red) and the instantaneous amplitude $A(t) = |f_0(t)|$ of its associated complex signal (in blue) for $t \in [-300, 500]$. The period of the amplitude function A is 200π, which is exactly the distance between two quiescent periods.

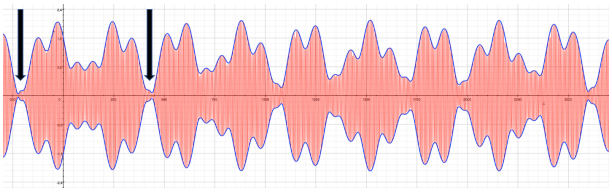

Figure 12: For the case displayed in Figure 10 on the right, this is the graph of the real signal $S(t)$ (in red) and the instantaneous amplitude $A(t) = |f_0(t)|$ of its associated complex signal (in blue) for $t \in [-300, 2700]$.

We finally discuss the "irrational" case, where the number $\varepsilon_3/\varepsilon_1$ is not a rational number. In this case, as opposed to the rational case, the trajectory of the complex signal $f_0(t)$ is not periodic. One easily verifies directly from its definition in (25) that the trajectory of $f_0(t)$ is contained in the complex annulus Ω given by

$$\Omega = \{z \in \mathbb{C} : \ |\alpha_1 - \alpha_3| \leq |z - \alpha_2 e^{i\phi_2}| \leq \alpha_1 + \alpha_3\}. \tag{28}$$

With some imagination, such an annulus can already be recognized in Figure 10 on the right. Indeed, if we change the value $\omega_1 = 0.951$ in the right example into an arbitrary

irrational number close to 0.951, the corresponding trajectory would "densely" fill the complete annulus Ω. This means that for each $z \in \Omega$, $T > 0$, $\varepsilon > 0$ there exists a time $t > T$ with $|f_0(t) - z| < \varepsilon$.

The existence of quiescent periods for the irrational case depends on the proximity of the origin to the annulus Ω. If the distance $d(0, \Omega)$ is small (which is the case, for example, if $0 \in \Omega$), there will exist infinitely many quiescent periods, but the spacing of these periods will be chaotic (as opposed to the regular spacing in the rational case). It easily follows from the definition of the annulus in (28) that the proximity criterion for the existence of quiescent periods is given by

$$|\alpha_1 - \alpha_3| \lesssim \alpha_2 \lesssim \alpha_1 + \alpha_3, \tag{29}$$

which is equivalent to the more symmetric condition that each of the numbers α_1, α_2, α_3 is (approximately) smaller than the sum of the other two. The latter condition can further be rewritten into the single condition

$$\max(\alpha_1, \alpha_2, \alpha_3) \lesssim \frac{1}{2}(\alpha_1 + \alpha_2 + \alpha_3). \tag{30}$$

4.6 The deterministic case for arbitrary n

We consider an arbitrary real signal S of the form (9) with angular frequencies $\omega_j > 0$, real amplitudes $\alpha_j > 0$ and phase shifts $\phi_j \in \mathbb{R}$. By renumbering we can assume without loss of generality that

$$\alpha_1 \geq \alpha_2 \geq ... \geq \alpha_n. \tag{31}$$

Setting $\omega = \omega_1$ and $\varepsilon_j = \omega_j - \omega_1$ $(j = 2, 3, ..., n)$, the complex signal $f_0(t)$ defined in (13) is given by

$$f_0(t) = \alpha_1 e^{i\phi_1} + \sum_{j=2}^{n} \alpha_j e^{i(\varepsilon_j t + \phi_j)}. \tag{32}$$

We make again a distinction between the "rational" and "irrational" case. In the rational case the numbers $\varepsilon_2, \varepsilon_3, ..., \varepsilon_n$ are rationally dependent, which means that there exist integers $k_2, k_3, ..., k_n$, not all zero, such that

$$k_2\varepsilon_2 + k_3\varepsilon_3 + ... + k_n\varepsilon_n = 0. \tag{33}$$

In the irrational case the numbers $\varepsilon_2, \varepsilon_3, ..., \varepsilon_n$ are rationally independent, which means that the only way for (33) to hold is that all integers $k_2, k_3, ..., k_n$ are zero.

We first deal with the **irrational case**. In that case it follows from Kronecker's theorem (Hardy and Wright, 1979, Theorem 444) that the trajectory of $f_0(t)$ is contained and densely fills the set

$$\Omega = \{\alpha_1 e^{i\phi_1} + \sum_{j=2}^{n} \alpha_j z_j : \ z_j \in \mathbb{C}, |z_j| = 1\}. \tag{34}$$

One easily verifies (with induction) that the set Ω is a (closed) annulus in the complex plane with center $z = \alpha_1 e^{i\phi_1}$ and (external/internal) radii given by

$$\begin{aligned} r_{\text{ext}} &= \alpha_2 + \alpha_3 + ... + \alpha_n \\ r_{\text{int}} &= \max(0, \alpha_2 - \alpha_3 - ... - \alpha_n). \end{aligned}$$

It follows that the distance from the origin to the set Ω is equal to

$$d(0, \Omega) = \max(0, \alpha_1 - \alpha_2 - ... - \alpha_n). \tag{35}$$

Since quiescent periods are periods in which $A(t) = |f_0(t)| \approx 0$, there exist quiescent periods if and only if $d(0, \Omega) \approx 0$, which is equivalent to the condition

$$\alpha_1 - \alpha_2 - ... - \alpha_n \lesssim 0.$$

Hence we have shown that in the irrational case there exist quiescent periods if and only if

$$\max(\alpha_1, \alpha_2, ..., \alpha_n) \lesssim \frac{1}{2}(\alpha_1 + \alpha_2 + ... + \alpha_n). \tag{36}$$

In the **rational case** (which should be seen as exceptional) the situation is slightly different. In that case the trajectory of $f_0(t)$ is still contained in the set Ω, but it does not densely fill that set. Hence condition (36) is necessary but not sufficient for the existence of quiescent periods.

4.7 Random sampling of signals for arbitrary n

We now turn to the case of an arbitrary number n of harmonics, still under the narrow-bandwidth assumption. The case of arbitrary n arises when representing a "general" signal with a certain given spectrum. In practice, e.g. for the simulation tool FREDYN, frequencies ω_j and complex amplitudes a_j are drawn randomly from a distribution modeled on the spectrum. Since the spectrum does not contain information about the phases, the phases are chosen following a uniform distribution.

We mimic this situation as follows. First we assume that a set of frequencies $\omega_j \in \mathbb{R}$, $j = 1, \ldots, n$ are *given*, once and for all. Next we assume that $a_1, \ldots, a_n$ are independent, centered, complex Gaussian random variables, i.e. $a_j \sim \mathcal{CN}(0, \sigma_j I_2)$, for some $\mathcal{C} > 0$ and $\sigma_j > 0$, where I_2 is the two-dimensional identity matrix. We then let f_0 be given by

$$f_0(t) = \sum_{j=1}^{n} a_j e^{i(\omega_j - \omega)t}. \tag{37}$$

The above-mentioned slower time scale of $f_0(t)$ corresponds to the fact that $|\omega_j - \omega| \leq \varepsilon \ll \omega$.

By choosing the coefficients to be random variables in $\mathbb{C}$, the functions f and f_0 become random variables in $L^\infty(\mathbb{R}; \mathbb{C})$; the assumption that the coefficients are *normal*

makes the functions f and f_0 *Gaussian processes.*[1] Because time translation corresponds to multiplying the coefficients by unit-length complex numbers, and because the coefficients are normally distributed with mean zero and isotropic covariance, the process is *stationary.*

4.8 The level-crossing approach for arbitrary n

The study of extremes of a stochastic process has been a topic of great interest in engineering. For stationary processes, the main tool has been Rice's formula for the expected number of level crossings Rice (1944) and its generalizations. The most recent account of this theory has been given by Lindgren (2013). For a Gaussian stationary process X_t with zero mean, as we're considering here, the number of upcrossings of the level $u > 0$ per unit time is given by

$$\mu^+(u) = \frac{1}{2\pi}\sqrt{\frac{\lambda_2}{\lambda_0}}e^{-u^2/(2\lambda_0)},$$

where $\lambda_k = \int_{-\infty}^{\infty} |\omega|^k \mathrm{S}(\omega)\,\mathrm{d}k$ are the spectral moments of X_t; here, if we choose $X = f$ as in (8), then we have

$$\lambda_k = \sum_{j=1}^{n} |a_j|^2 |w_j|^k.$$

The up-crossings of the mean level define the *mean period* $T_2 = 1/\mu^+(0) = 2\pi\sqrt{\lambda_0/\lambda_2}$.

Using this approach, Cramér and Leadbetter (1967) have studied the following problem: A process X_t is said to *fade* below a level u if the envelope R_t of X_t has a downcrossing of the level u. The *length of the fade* is the time between a downcrossing and the next upcrossing of the level u by R_t. This corresponds closely to our notion of a quiescent period (for a single variable, e.g. the heave signal).

Let us quote Lindgren here (Lindgren, 2013, p261): *'One of the most intriguing problems in stationary process theory is that of the distribution of the length of excursions above a critical fixed level. Even for Gaussian processes, no explicit solution is known, except in a few cases.'* However, Lindgren then goes on to present *'a method to numerically calculate the* exact *distributions of excursion length'*, based on the evaluation of an infinite dimensional expectation for the so-called Slepian model. Unfortunately this is beyond the scope of this report, but could be very useful for the first problem posed by MARIN. Some of the numerical calculations are available in the WAFO Matlab toolbox The WAFO group (2011).

Generalizing the analysis to vector processes, Lindgren even mentions the phenomenon of *the seventh wave*, i.e. "the observation that waves on a shore or on the ocean seem to have a typical regularity of one big wave followed by six smaller ones" (Lindgren, 2013, p.271). The expected number of u-upcrossings of the envelope $R(t)$

[1] A Gaussian process is a stochastic process whose finite marginals are distributed according to multivariate normal distributions.

per unit time interval is given by

$$\mu_R^+(u) = \sqrt{\frac{\lambda_2(1-\rho^2)}{2\pi\lambda_0}}\frac{u}{\sqrt{\lambda_0}}e^{-u^2/(2\lambda_0)},$$
$$= \sqrt{\frac{\lambda_0\lambda_2-\lambda_1^2}{2\pi\lambda_0^3}}ue^{-u^2/(2\lambda_0)},$$

where $\rho^2 = \lambda_1^2/(\lambda_0\lambda_2)$ is the squared correlation between Hilbert transform and derivative of the process. The inverse of this corresponds to the result given by Cramér and Leadbetter (1967) for the mean length of a fade. And the average number of envelope u-upcrossings per mean period is

$$T_2\mu_R^+(u) = \sqrt{2\pi(1-\rho^2)}\frac{u}{\sqrt{\lambda_0}}e^{-u^2/(2\lambda_0)},$$

and this corresponds to the inverse of the average number of waves per envelope upcrossing.

4.9 Alternative estimates for arbitrary n

In this report we also derive a different type of estimate. As remarked above, the modulus $|f(t)|$ equals the modulus $|f_0(t)|$ for all t. We exploit this by choosing the norm $\|f\|_{[t,t+\tau]}$ in Definition 4.1 to be the sup-norm of f on $[t,t+\tau]$, i.e. $\|f\|_{L^\infty(t,t+\tau)} := \sup_{s\in[t,t+\tau]}|f(s)|$. Then, it follows that $\|f\|_{L^\infty(t,t+\tau)} = \|f_0\|_{L^\infty(t,t+\tau)}$; also, since the process is stationary, the distribution of $\|f\|_{L^\infty(t,t+\tau)}$ is independent of t, so that $\mathbb{E}(\|f\|_{L^\infty(t,t+\tau)})$ is independent of t. In this context we interpret the "average" mentioned in Definition 4.1 as this expectation.

Then the probability of a quiescent period of length τ at time t equals

$$\mathbb{P}\Big(\|f\|_{L^\infty(t,t+\tau)} \le \theta\mathbb{E}(\|f\|_{L^\infty(t,t+\tau)})\Big) = \mathbb{P}\Big(\|f_0\|_{L^\infty(t,t+\tau)} < \theta\mathbb{E}(\|f_0\|_{L^\infty(t,t+\tau)})\Big), \tag{38}$$

and as we already mentioned this probability is independent of t.

As it is difficult to analyse $\|f_0\|_\infty$ directly, we first focus on the L_2-norm $\|f_0\|_2^2 := \|f_0\|^2_{L^2(t,t+\tau)} := \int_t^{t+\tau}|f_0(t')|^2\,dt' \le \tau\|f_0\|^2_{L^\infty(t,t+\tau)}$. We prove the following theorem:

Theorem 4.2 (Estimate of the distribution of the L^2-norm)**.** *Let f_0 be the Gaussian process that we construct above, and assume that $\varepsilon \ll 2\pi/\tau$. Then*

$$\mathbb{P}\Big(\|f\|^2_{L^2(t,t+\tau)} \le \theta^2\mathbb{E}(\|f\|^2_{L^2(t,t+\tau)})\Big) \approx 1-e^{-\theta^2}. \tag{39}$$

Note that the condition $\varepsilon \ll 2\pi/\tau$ is stronger than the earlier narrow-bandedness assumption $\varepsilon \ll \omega = 2\pi/T$, whenever $\tau > T$ (see the discussion on page 14). Under this assumption, over an interval $(t,t+\tau)$, the signal looks like a single harmonic (whose amplitude and phase can be viewed both as random for fixed t, or alternatively as t-dependent for each realization).

Proof. The L^2-norm of f_0 is readily computed. We have

$$\|f_0\|^2_{L^2(0,\tau)} = \int_0^\tau f_0(s)\overline{f_0(s)}\,ds = \sum_{j,k=1,\dots,n} a_j\overline{a_k}\int_0^\tau e^{i(\omega_j-\omega_k)s}\,ds = \sum_{j,k=1,\dots,n} A_{jk}\,a_j\overline{a_k},$$

where

$$A_{jk} = \int_0^\tau e^{i(\omega_j-\omega_k)s}\,ds = \begin{cases} \frac{1}{i(\omega_j-\omega_k)}\cdot\left(e^{i(\omega_j-\omega_k)\tau}-1\right) & j\neq k \\ \tau & j=k. \end{cases}$$

Since $\varepsilon \ll \omega$, we replace A_{jk} by its limit τ, i.e. $A_{jk}=\tau$ for all j,k. Then

$$\|f_0\|_{L^2(0,\tau)} = \tau\left|\sum_{j=1}^n a_j\right|^2.$$

Next we determine the distribution of $|\sum_{j=1}^n a_j|^2$. Note that the a_j's are assumed to be independent and centered complex Gaussian variables with variance matrices $\sigma_j^2 I_2$, and therefore we have:

$$\sum_{j=1}^n a_j \sim \mathcal{CN}(0,\sigma^2 I_2),$$

where $\sigma^2 = \Sigma_{j=1}^n \sigma_j^2$. It follows that:

$$\left|\sum_{j=1}^n a_j\right|^2 \sim \sigma^2\cdot(Z_1^2+Z_2^2) \sim 2\sigma^2\cdot Z,$$

where Z_1, Z_2 are independent, standard normal random variables and Z follows a standard exponential distribution (the sum of the squares of two independent standard normal random variables is exponentially distributed with mean 2). In other words, the squared norm $\|f_0\|^2_{L^2(t,t+\tau)}$ follows an exponential distribution with parameter $2\tau\sigma^2$.

Therefore, using the formula for the exponential cumulative distribution function we obtain:

$$\begin{aligned}\mathbb{P}\Big(\|f\|^2_{L^2(0,\tau)} < \theta^2\mathbb{E}\|f\|^2_{L^2(0,\tau)}\Big) &= \mathbb{P}\Big(\|f_0\|^2_{L^2(0,\tau)} < \theta^2\mathbb{E}\|f_0\|^2_{L^2(0,\tau)}\Big) \\ &\approx \mathbb{P}\left(\tau\Big\|\sum_{j=1}^n a_j\Big\|_2 < 2\theta^2\tau\sigma^2\right) = 1-e^{-\theta^2}.\end{aligned}$$

□

If we prefer to have an estimate of the norm $\|f\|_{L^\infty(t,t+\tau)} = \|f_0\|_{L^\infty(t,t+\tau)}$, then we can use the Gagliardo-Nirenberg interpolation inequality (Nirenberg, 2011) to derive this from the previous estimate. This inequality gives an estimate of the supremum norm in terms of the L^2-norms of f_0 and f_0'. Although there are various versions in the literature, we prove our own because it gives us control over the constants:

Lemma 4.3. *For any $f \in C^1([0,\tau];\mathbb{C})$,*

$$\frac{1}{\tau}\|f\|^2_{L^2(0,\tau)} \le \|f\|^2_{L^\infty(0,\tau)} \le \frac{2}{\tau}\|f\|^2_{L^2(0,\tau)} + \tau\|f'\|^2_{L^2(0,\tau)}. \tag{40}$$

Proof. The first inequality is immediate. For the second, we write for any $s,t \in [0,\tau]$

$$|f(t)|^2 = |f(s)|^2 + 2\,\mathrm{Re}\int_s^t f(\sigma)f'(\sigma)\,d\sigma \le |f(s)|^2 + \frac{1}{\tau}\|f\|^2_{L^2(0,\tau)} + \tau\|f'\|^2_{L^2(0,\tau)}.$$

Integrating left and right over $s \in [0,\tau]$, and taking the supremum over $t \in [0,\tau]$, we find

$$\tau\|f\|^2_{L^\infty(0,\tau)} \le \int_0^\tau |f(s)|^2\,ds + \|f\|^2_{L^2(0,\tau)} + \tau^2\|f'\|^2_{L^2(0,\tau)} = 2\|f\|^2_{L^2(0,\tau)} + \tau^2\|f'\|^2_{L^2(0,\tau)}.$$

This proves the result. □

From this inequality we deduce the following theorem.

Theorem 4.4 (Estimates of the distribution of the infinity-norm)**.** *Assume the same conditions as Theorem 4.2. Setting $\tilde\theta^2 := \theta^2\tau^{-1}\mathbb{E}(\|f\|^2_{L^2(t,t+\tau)})$, we have*

$$\mathbb{P}\Big(\|f_0\|^2_{L^\infty(t,t+\tau)} \le \tilde\theta^2\Big) \lesssim 1 - e^{-\theta^2}$$
$$\mathbb{P}\Big(\|f_0\|^2_{L^\infty(t,t+\tau)} \le \tilde\theta^2\Big) \gtrsim 1 - e^{-\theta^2/2}.$$

Note the scaling of $\tilde\theta$: since $\|\cdot\|_2^2$ scales as τ, and $\|\cdot\|_\infty$ scales as 1, we rescale the L^2-norm by τ in the definition of $\tilde\theta$ in order to make $\tilde\theta$ τ-invariant.

Proof. Above we already calculated that

$$\|f_0\|_2^2 = \sum_{j,k=1,\dots,n} A_{jk}\,a_j\overline{a_k}.$$

Similarly, we see that

$$\|f_0'\|_2^2 = \sum_{j,k=1,\dots,n} a_j\overline{a_k}\,i(\omega_j-\omega)\overline{i(\omega_k-\omega)}\int_0^\tau e^{i(\omega_j-\omega_k)s}\,ds = \sum_{j,k=1,\dots,n} \widetilde{A}_{jk}\,a_j\overline{a_k},$$

where

$$\widetilde{A}_{jk} := (\omega_j-\omega)(\omega_k-\omega)A_{jk}.$$

Therefore, using Lemma 4.3,

$$\sum_{j,k=1,\dots,n} A_{jk}\,a_j\overline{a_k} \le \tau\|f_0\|^2_{L^\infty(0,\tau)} \le \sum_{j,k=1,\dots,n} B_{jk}\,a_j\overline{a_k},$$

where $B = 2A + \tau^2 \widetilde{A}$, i.e. $B_{jk} = (2 + \tau^2(\omega_j - \omega)(\omega_k - \omega))A_{jk}$.

As before we use the narrow-bandedness assumption that $\varepsilon \ll 2\pi/\tau$, which implies that $A_{jk} \approx \tau$ and $B_{jk} \approx 2A_{jk} \approx 2\tau$; then the inequalities above reduce to

$$\left|\sum_{j=1}^{n} a_j\right|^2 \leq \|f_0\|^2_{L^\infty(0,\tau)} \leq 2\left|\sum_{j=1}^{n} a_j\right|^2.$$

In the proof of Theorem 4.2 we already observed that $|\sum_{j=1}^{n} a_j|^2$ is exponentially distributed with parameter $2\sigma^2$; therefore

$$\mathbb{P}\Big(\|f_0\|^2_{L^\infty(t,t+\tau)} \leq \tilde{\theta}^2\Big) \leq \mathbb{P}\left(\left|\sum_{j=1}^{n} a_j\right|^2 \leq \tilde{\theta}^2\right) \approx 1 - e^{-\tilde{\theta}^2/2\sigma^2},$$

and

$$\mathbb{P}\Big(\|f_0\|^2_{L^\infty(t,t+\tau)} \leq \tilde{\theta}^2\Big) \geq \mathbb{P}\left(2\left|\sum_{j=1}^{n} a_j\right|^2 \leq \tilde{\theta}^2\right) \approx 1 - e^{-\tilde{\theta}^2/4\sigma^2}.$$

The assertion of the theorem follows from remarking that $\tilde{\theta}^2 = \theta^2 \tau^{-1} \mathbb{E}\|f_0\|^2_{L^2(0,\tau)} = \theta^2\, 2\sigma^2$. □

4.10 Discussion

The various results mentioned above all give partial characterizations of the probability of the appearance of quiescent periods in a narrow-banded signal.

The small-n results illustrate how quiescent periods may or may not recur in deterministically chosen sums of harmonics, and show how a precise characterization quickly becomes complex as the number n of harmonics increases.

Turning to arbitrary n, by choosing random coefficients, with uniformly distributed phases and normal amplitudes, we can leverage the property that the signal is a Gaussian process to characterize rates of upcrossings; possibly the Slepian-model can lead to a more precise characterization of the distribution of quiescent periods.

We also derived some estimates of our own for the probability distribution of quiescent periods defined by the L^2 and the L^∞ norm, under the assumption of strong narrow-bandedness. Although each of these various results covers only part of the picture, together they do give some insight into the occurrence of quiescent periods in sums of harmonics.

5 Deterministic and stochastic models for prediction of QPs

As a second main step, MARIN would like to help the HLO to predict quiescent periods with high confidence. We pursued several approaches to this problem, by both

deterministic and stochastic models, with different levels of success. The underlying hope is that the signal in a finite time interval contains enough information to allow for forecasts in the very near future. This means that certain patterns are repeating in the ship motion.

5.1 Fourier continuation of the signal

The ship motion is assumed to be a second-order stationary stochastic process X_t that can be described by a continuous spectrum $S(f)$. In fact, as the sea surface elevation can be considered a Gaussian process, and the ship dynamics can be assumed to be linear, the resulting ship motion reponse is also a Gaussian process. In simulations, e.g. the ones performed by MARIN, realizations of this process are generated in the form of time series that share the same second-order statistical properties. The most common method is superposition of a large number of frequency components with randomized phases

$$f(t) = \sum_k \sqrt{2S(\omega_k)\Delta\omega_k}\cos(\omega_k t + \delta_k), \tag{41}$$

where δ_k are drawn from the uniform distribution on the interval $[0, 2\pi]$. This method can be readily extended to the multivariate setting Shinozuka and Jan (1972). Mathematically, there is thus a difference between the simulated signals and ship motions that are measured in reality.

Nevertheless, in both cases the underlying structure of the signals suggests that Fourier analysis might be a useful tool to understand – and possibly predict – the signals in question. Naively, one would suspect that if one estimated the Fourier decomposition of the signal, i.e. the frequencies, amplitudes and phase angles, one could simply continue the signal and predict its future evolution. For example, in Eq. 41 the randomness appears only in the phases. Each realization of this process, however, is a deterministic function. Of course, for real-world data the situation is more unclear, but let us focus on the simpler case of simulated data for now.

The main difficulty in practice is that such an analysis is based only on a finite time series $(x_0, x_1, \ldots, x_{n-1})$, whereas the underlying signal is defined on all of $\mathbb{R}$. The discrete Fourier transform can be used to estimate the frequency components of the signal, but it is essentially a Fourier series. Since Fourier series of a non-periodic function are really the Fourier series of the periodic extension of the function, this assumes that the past history of the ship motion $(x_0, \ldots, x_{n-1})$ is repeated periodically. In other words, prediction based on Fourier continuation of the signal consists of trivially repeating the signal from the start of the analysis period. This is illustrated in Fig. 13. The continuation therefore depends on the length of the past history that is used. It is not clear how this can lead to a usable predictor of future ship motions. One might average over different lengths of the past of the signal, but the resulting variance in the prediction is too large to be useful.

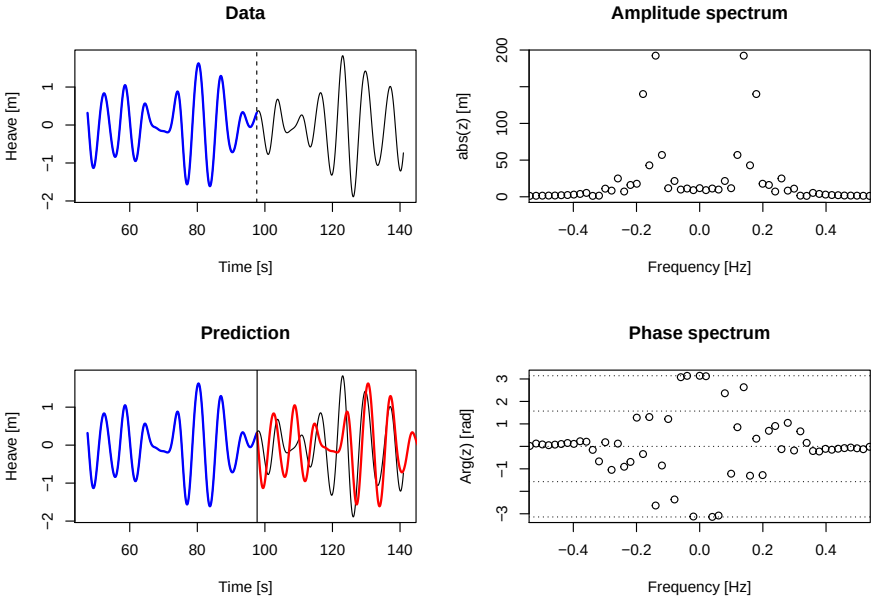

Figure 13: Discrete Fourier transform of ship heave signal. Prediction is based on periodic continuation of the signal (see text).

5.2 Prediction in stationary processes

Prediction in stationary processes has been studied already by Kolmogorov. A very accessible introduction is given by Fristedt et al. (2007). An extensive treatment was given in Yaglom (1962), and the following is simply an application of his approach. Let us consider here the *extrapolation problem* for a stationary random sequence $(x_i)_{t\in\mathbb{Z}}$, with the *mean square extrapolation error* as error criterion. This is the problem of minimizing

$$\sigma^2_{m,n} = E\left[|x_{t+m} - g(x_{-1}, x_{-2}, \dots x_{-n})|^2\right] \tag{42}$$

over all extrapolation functions g. We restrict ourselves here to the class of linear extrapolation functions

$$g(x_{-1}, x_{-2}, \dots, x_{-n}) = \alpha_1 x_{-1} + \alpha_2 x_{-2} + \cdots + \alpha_n x_{-n}.$$

If the sequence x_i is a Gaussian process (which can be assumed here) this is no restriction: it can be shown that in this case the best linear extrapolation formula coincides with the best possible extrapolation formula (Yaglom, 1962, ch.20).

Let us assume that we know the the correlation function

$$C(j,i) = E[x_j x_i]$$

of the sequence x_i. Because of stationarity, this does not depend on time i, but only on the *lag* $k = j - i$, such that

$$C(k) = E[x_{i+k} x_i]$$

for any $i \in \mathbb{Z}$.

The normal equations corresponding to the minimization problem in Eq. 42 are

$$\left.\frac{\partial \sigma^2_{m,n}}{\partial \alpha_k}\right|_{\alpha_1 = a_1, \ldots, \alpha_n = a_n} = -C(m+k) + \sum_{i=1}^{n} a_i C(k-i) = 0 \quad (k = 1, 2, \ldots, n). \quad (43)$$

This is simply a linear system of n equations in n unknowns, which under the conditions assumed here always has a unique solution. The best linear extrapolation formula is then

$$\hat{x}_{t+m} = a_1 x_{t-1} + a_2 x_{t-2} + \cdots + a_n x_{t-n}$$

and the corresponding mean square error is given by

$$\sigma^2_{m,n} = C(0) - \sum_{k=1}^{n} \alpha_k C(m+k).$$

Yaglom remarks that this approach is impractical since the solution of Eq. 43 is tedious for $n > 10$ and continues to develop a spectral theory of the solution, applicable whenever the correlation function or spectral density is a known rational function, as well as the theory for the case of continuous time. However, this was written at a time when mainframe computers had only 10 KB of memory. For our purposes, the above approach seems the most direct and useful.

Testing this approach with the time series consisting of the extrema of the heave signal, we start by looking at the autocorrelation function in Figure 14. The alternating nature of the extrema process hides the relevant information, and it becomes more natural to consider the absolute extrema. It can be seen that after about 4 values the absolute extrema are not correlated anymore, within the estimated statistical uncertainty. Note that we removed the mean of the signals before the analysis, so subsequent results are for zero-mean processes.

Setting up the linear prediction for the absolute extrema process is straightforward. Figure 15 shows the one-step ahead prediction (top) and the three-step ahead prediction (bottom). As expected for this linear method, the n-step ahead prediction approaches the mean value (of zero) for increasing n, and the prediction becomes less reliable.

Figure 16 gives an indication of the accuracy of prediction that can be achieved with this method, in terms of root mean square error between prediction and known signal. It can again be seen that prediction beyond 4 steps ahead (amounting to about two waves) is not really possible.

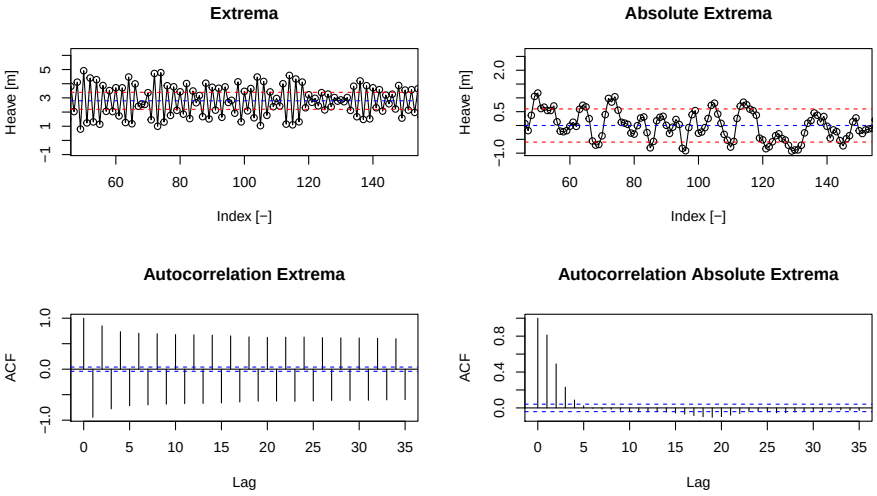

Figure 14: Autocorrelation of extrema process and absolute extrema process.

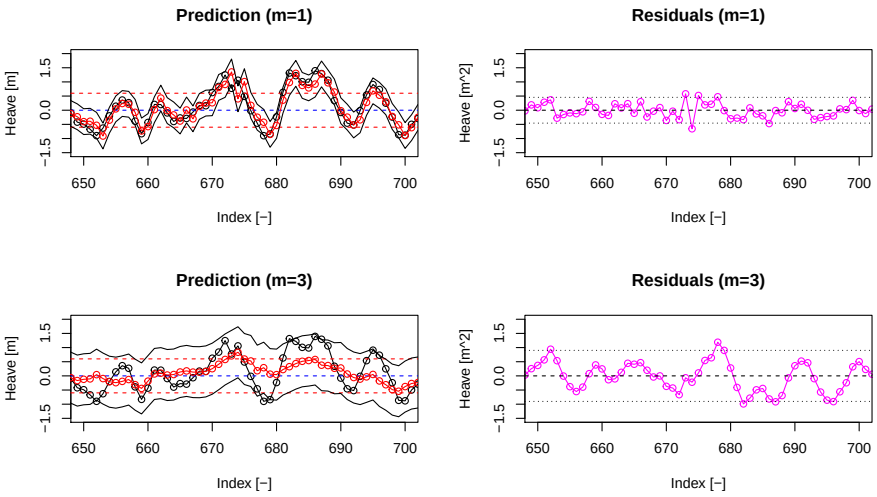

Figure 15: Linear prediction of absolute extrema process. An example for two different values of the step ahead m are shown. In both cases a long history ($n = 400$) was used. Root mean square error estimates are shown in addition.

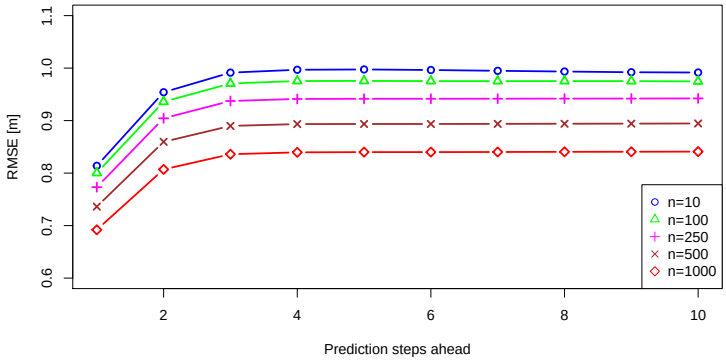

Figure 16: Accuracy of linear prediction for different lengths n of past history. Root mean square error (RMSE) against number of prediction steps.

5.3 Statistical modeling of ship movements

In this section we consider the approach of fitting a stochastic model to the data on ship movements that can be used to predict or test for the occurrence of a quiescent period. In practice, the HLO appears to base his decision as to when to call the helicopter in for a landing attempt on the ship movements that occurred during the recent past. This suggests that it ought to be possible to predict the occurrence of a quiescent period based on past observations. In this section we concentrate on linear models, and outline some preliminary ideas on which models may be useful. We focus on the modeling of the wave envelope by considering observations of the ship motion of the recent past.

In Section 5.3.1 we consider *autoregressive moving average* (ARMA) models, which are commonly used to model economic time series but have widespread applications in other areas (Brockwell and Davis, 2009). We also provide a preliminary example in which we fit an ARMA model to the sequence of extrema of the heave data set provided by MARIN. In Section 5.3.3 we explain how one can use sequential hypothesis testing as an aid to decide whether or not a quiescent period has commenced, given a fitted ARMA model. In Section 5.3.2 we propose a variant of a *logistic regression* model as a possible improvement to the ARMA model for the problem at hand. We provide a brief summary in Section 5.3.4.

5.3.1 Autoregressive Moving-Average model

The basic ARMA model is defined as follows. We assume time is slotted into time epochs of equal length that we index by $t \in \mathbb{N}$. Let $(Z_t) \in \mathbb{R}^d$ denote a sequence of

Gaussian independent and identically distributed (i.i.d.) random variables with zero mean and variance σ^2. Such a sequence is often referred to as *white noise process*. Suppose the data sequence of interest is a realization of a stochastic process $(X_t) \in \mathbb{R}^d$. Then the process is referred to as ARMA(p,q) process if it satisfies the recursion

$$X_t = c + \sum_{i=1}^{p} A_i X_{t-i} + \sum_{j=0}^{q} B_j Z_{t-j}, \tag{44}$$

where $c \in \mathbb{R}$, and A_i and B_j are coefficient matrices of suitable dimensions. For background on ARMA modeling see, for example, Brockwell and Davis (2009).

It is a virtue of the ARMA model that forecasting based on this model is particularly easy. Given the observations up to time t, we can predict the next vector of data points by

$$\hat{X}_t = c + \sum_{i=1}^{p} A_i x_{t-i} + \sum_{j=1}^{q} B_j z_{t-j},$$

where we have replaced Z_t by its expected value zero. Thus, the model can be used to predict the magnitude of the ship movements in the near future.

We now provide a small example where we fitted a univariate ARMA model to the series of heave data. We focussed on this data series because the magnitude of consecutive heave movements seems to be particularly important for the decision of the HLO to initiate a landing attempt. We expect, however, that the predictive capability of the model can be improved by including other relevant time series.

First, we recall that the relevant information for predicting a quiescent period is included in the envelope. We therefore extract the sequence of local extrema of the heave data series. We then take the absolute value of the extrema and center the resulting time series by subtracting the mean value: indeed, the amplitude is what affects the helicopter landing.

To estimate the model parameters, we used the package "forecast" in the statistical computing language R. We fitted the model to a training set of 200 data points, resulting in an ARMA(2,0). With this model specification and the estimated coefficients, we ran diagnostic tests on the residuals to verify that the latter are Gaussian white noise. We then used the model to predict the subsequent 10 data points, see Fig. 17.

We remark that the accuracy of the prediction did not improve with a larger training set; seemingly, the series can be modeled as ARMA only locally. Further testing with multivariate ARMA is needed to optimize the data to be included in the model: we included only the extrema of the heave data series, but other data such as roll and pitch motion may be significant as well. It is also possible to attempt to model the amplitude of the wave heaves rather than the absolute value of each extreme point as we did in this preliminary experiment. It may also be that predicting the actual value of the time series based on simple linear models is not possible with sufficient accuracy. In the next section therefore we suggest a logistic regression model that can be used to decide whether or not a quiescent period has commenced or is about to commence.

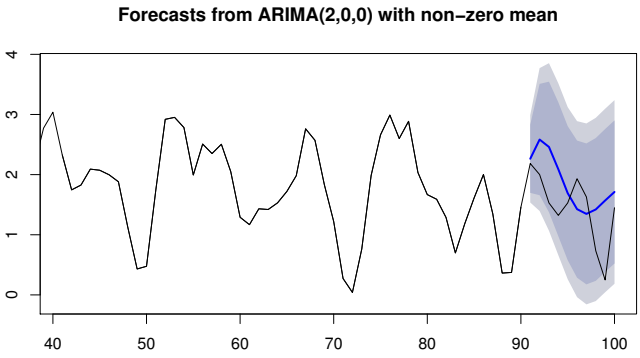

Figure 17: Example of a forecast for heave extrema based on an ARMA(2,0). The shaded area indicates the 90% (dark grey) and 95% (light grey) confidence intervals.

5.3.2 Logistic regression

In the preliminary experiment we presented in Section 5.3.1, the forecasts we obtained with the ARMA model corresponded to rather large confidence intervals. We suggested a number of steps that may help to remedy this issue. Note, however, that our objective is to decide whether or not to expect a quiescent period; predicting the actual value of the time series is not strictly necessary for this purpose. As an alternative to the ARMA model we therefore propose the following *logistic regression* model.

Let Y denote a random variable taking values in $\{0, 1\}$, where the realization 1 indicates that the current time period is quiescent. Let π denote the probability that $Y = 1$. We now seek to explain the realization of π by current and past observations. For example, consider

$$\log\left(\frac{\pi}{1-\pi}\right) = \sum_{j=1}^{p}\sum_{i=0}^{k} \beta_{i,j} X_{i,t-j}, \tag{45}$$

where $\beta_{i,j}$ denote the coefficients. Here, $X_{i,t-j}$ denotes the random variable corresponding to an observation obtained at time $t-j$ of a particular type of ship movement labelled by i.

A simple logistic regression model can be estimated using maximum likelihood techniques that are readily available in any standard statistical programming language; see (Kabacoff, 2015, Section 13.2) for an example using R. Note, however, that the sequence $(X_{i,t-j})_j$ is not independent; therefore care has to be taken that the correlation between included variables is not too strong. If variables are nearly perfectly correlated, the matrix of coefficients is nearly singular, which can lead to

problems with standard estimation procedures (this is known as *multicollinearity*).

In order to estimate a model for explaining Y, we need to label each data point of the training set by 1 or 0 depending on whether or not it lies within a quiescent period. We remark that for a period to qualify as quiescent, it must be of sufficient length, $T = 5$ say. Thus, if we collect measurements every Δ time units, where $\Delta < T$, then, we must observe nearly perfect positive correlation between values of Y_t: If $Y_t = 1$ then we must have that neighbouring points also have realization 1. Furthermore, Y_t is not necessarily measurable at time t: We only know whether or not we should label Y_t as quiescent after we observed a period of length T, during which the waves were quiet. Suppose, for example, that $\Delta = 1/T$ and consider the first observation we collect (at time Δ, that is), which we denote by Y_Δ. Then we need to observe $T - 1$ more data points before we can determine whether Y_Δ is part of a quiescent period. Therefore, we cannot use Y_Δ to predict the value of $Y_{2\Delta}$, say. This explains why we did not include past observations Y_t as explanatory variables on the right-hand side of (45).

A possible alternative is to group data into sliding windows such that for each new observation arriving the oldest observation is discarded. If the size of the windows coincides with the minimum length of a quiescent period, then windows are not perfectly correlated, and we can determine whether or not the previous window was quiescent, namely, if all observations in the previous window corresponded to a quiescent period. This alternative framework leads to a model of the form

$$\log\left(\frac{\pi}{1-\pi}\right) = \sum_{j=1}^{p}\sum_{i=0}^{k}\beta_{i,j}X_{i,t-j} + \sum_{k=1}^{q}\gamma_k Y_{t-k}^{w}, \tag{46}$$

where Y_t^w denotes the random variable describing whether or not the collection of data points belonging to the window that ends at time t.

To gain more certainty as to whether or not a quiescent period has commenced, the predicted future values of the relevant time series may be supplemented by the outcome of a statistical hypothesis test. We briefly discuss such a procedure in the next section for the ARMA model example.

5.3.3 Change point detection

In this section we explain how change point detection procedures can be applied to test a stationary ARMA time series for a change in the mean value. Specifically, we focus on the popular CUSUM method that was originally suggested by Page (1954). Similar procedures have been considered in Basseville and Nikiforov (1993); Chen and Gupta (2012); Robbins et al. (2011).

First, note from Eq. (44) that setting the initial white noise terms equal to zero, the sequence of residuals can be extracted from the sequence of observations as

$$\hat{Z}_t = x_t - c - \sum_{i=1}^{p} A_i X_{t-i} - \sum_{j=1}^{q}\hat{Z}_{t-j}.$$

A shift in the mean value of size μ in the sequence of observations therefore results in a shift in the mean value of the *innovations* $\hat{Z}_t$. Apart from the jump in the mean value, this sequence is i.i.d. Gaussian, so that we can focus on the easier problem of testing a sequence of independent Gaussian random variables. For further details on this and a comparison to the approach of testing the sequence of observations directly, see Basseville and Nikiforov (1993); Kuhn et al. (2014); Robbins et al. (2011).

The CUSUM method is essentially a sequential application of a log-likelihood ratio test. Consider testing the data in sliding windows of fixed size n. We wish to test whether at any time within the window the mean value of the sequence (Z_t) has changed from θ_0 to θ_1, say. Denote the hypothesis that such a change in mean has occurred at time k by $H_1(k)$. Thus, under $H_1(k)$ we have $\mathbb{E}[Z_t] = \theta_0$ for $t < k$ and $\mathbb{E}[Z_t] = \theta_1$ otherwise. Instead, under the null hypothesis H_0 we have $\mathbb{E}[Z_t] = \theta_0$ for all $t \in \{1, \ldots, n\}$.

Denoting by p_θ a normal density with mean θ, the log-likelihood ratio test statistic for testing the first window is

$$S_k := \sum_{t=k}^{n} Y_t := \sum_{t=k}^{n} \log \left(\frac{p_{\theta_1}(\hat{Z}_t)}{p_{\theta_0}(\hat{Z}_t)} \right)$$

(note that $Y_t = 0$ for $t < k$ since for such t the distribution of Z_t is equal under H_0 and $H_1(k)$). Obviously, the ratio of likelihoods $p_{\theta_1}(\hat{Z}_t)/p_{\theta_1}(\hat{Z}_t)$ is large if $p_{\theta_1}(\hat{Z}_t) > p_{\theta_1}(\hat{Z}_t)$, that is, if it is more likely to observe $\hat{Z}_t$ assuming that $H_1(k)$ is true. We would thus decide in favor of $H_1(k)$ if the test statistic S_k is large in some sense.

In order to decide whether a change point has occurred at some point k within the current window, we therefore need to check whether there is a $k \in \{1, \ldots, n\}$ such that S_k exceeds a certain critical value, b, say. As a result, the statistic for the *composite* test (that is, H_0 versus $\bigcup_{i=1}^{k} H_1(k)$) is

$$t_m := \max_{k \in \{m-n+1, \ldots, m\}} S_k(m), \tag{47}$$

where m is the label of the current window, and $S_k(m)$ denotes the test statistic corresponding to the innovations in the m-th window. Then, for a given threshold $b > 0$, the CUSUM method raises an alarm (indicating that a change has occurred) at time t_a, with

$$t_a := \inf \left[m : t_m \geq b \right]. \tag{48}$$

The name of the test is explained by noting that the test statistic t_m can be rewritten in terms of the cumulative sums $T_k := \sum_{t=1}^{k} \log p_{\theta_1}(\hat{Z}_t)/p_{\theta_0}(\hat{Z}_t)$ as follows,

$$t_m = T_m - \min_{k \in \{m-n+2, \ldots, m\}} T_{k-1}.$$

This is convenient with respect to computational efficiency since T_m equals $T_{m-1} + Y_m$, and computing $\min_{k \in \{m-n+2, \ldots, m\}} T_{k-1}$ only involves comparing the minimum computed at time $m-1$ with T_{m-1}. The choice of the threshold b can be based on simulation, or using approximations to the false alarm probability (see Kuhn et al. (2016)). For an example with multivariate data sequences see Kuhn et al. (2014).

5.3.4 Summary

The methods suggested in this section require more extensive testing. In particular, for the ARMA modelling approach other variables should be included besides the extrema of the heave movements. The logistic regression approach may be more suitable given that the objective is to discern between quiescent and non-quiescent periods, and should also be investigated based on numerical experiments. As suggested, one may use a change-point-detection procedure as a further indicator as to whether a quiescent period has commenced. Assuming that the HLO is risk averse, we would recommend that a quiescent period is then only announced if both the test and the predicted values indicate that such a period has started.

5.4 Short-term forecasting

In this section we will investigate a possibility of short-term forecasts of quiescent periods by solely analysing the ship motion data. That is to say we regard the motion data as a discrete-time stochastic process with memory. In this process, the states at time points $t_i,\ i \geq 0$ are correlated with the previous states at $t_{i-1}, t_{i-2}, \ldots, t_{i-k},\ 0 < k < i$. Since the original motion data is not supplied in a form of discrete states but as samples of a continuous-time function, one needs to convert the sampled signal into a discrete time series first. All in all, three questions crystallise as central to this analysis:
1) How to define patterns in data?
2) What correlation between the patterns is observable?
3) How good are the forecasts that can be made on the basis of observed patterns?
Let $f(t) \in C^2[0,\infty)$ represent one component of the measured signal. Without loss of generality we assume the signal $f(t)$ has zero mean value, $\int_0^\infty f(t)\,\mathrm{d}t = 0$. Furthermore, for the sake of simplicity we restrict our attention to local extrema of $f(t)$, that are in view of the smoothness class isolated points,

$$F = \left\{ f(t) : \frac{\mathrm{d}}{\mathrm{d}\xi}|f(\xi)|_{\xi=t} = 0 \text{ and } \frac{\mathrm{d}^2}{\mathrm{d}^2\xi}|f(\xi)|_{\xi=t} < 0 \right\}.$$

Occurrence times t naturally induce a strict order on F which allows us to speak of a sequence $F_i,\ i = 1, 2, \ldots$ In this way, each peak is characterised by a couple $(F_i, T_i) \in (0,\infty)^2$, and the whole signal by a sequence of peaks: $S = ((F_1, T_1), (F_2, T_2), \ldots)$, where F_i denotes the peak height and $T_i = \frac{t_{i+1} - t_{i-1}}{2}$ the duration. Furthermore, a configuration for d consecutive peaks, that is a d-tuple $s = ((F_1, t_1), \ldots, (F_d, t_d))$, is a point in $\Omega = (0,\infty)^{2d}$. We will now consider the probability space $(\Omega, \mathcal{F}, \mu_F),\ \mathcal{F} = 2^\Omega$, containing the d-tuples as outcomes. For given $p \in \mathcal{F}$, the probability measure $\mu_F\, p$ tells us how often the elements of p occur in the signal,

$$\mu_F\, p := \lim_{n\to\infty} \frac{1}{n-d} \sum_{i=d}^{n} \mathbf{1}_p(S_{i-d:i}),$$

where $S_{i-d:i}$ denotes a fragment of the signal S, and $\mathbf{1}_p$ is the indicator function for event p. Some events form $\mathcal{F}$ can be represented as a union tensors products. Let,

$$P^d = \left\{ \bigcup_{i=1}^{m} p_i : p_i \in \bigotimes_{j=1}^{d} [a_j, b_j], 0 < a_j < b_j \right\} \subset \mathcal{F}.$$

We refer to events $p = p_0 \times p_1,\ p_0 \in P^{d_1}, p_1 \in P^{d_2},\ d_1 + d_2 = d$ as patterns. For each pattern p there is a signal F such that $\mu_F\, p > 0$, which is not generally the case for events that are not patterns. For a given pattern p, we will now quantify its suitability for forecasting. Suppose one finds a d_0-tuple representing p_0 in the data. Is the expectation that a d_1-tuple from p_1 will follow immediately after a good forecast? Formally, the answer to this question unfolds into three distinct statistical estimates:
a) probability to find p_0, is simply given by $P_0(p) = \mu_F\, p_0$;
b) probability that p_0 is followed by p_1, $P_1(p) = \frac{\mu_F\, p}{\mu_F\, p_0}$;
c) probability that p_1 is preceded by p_0, $P_2(p) = \frac{\mu_F\, p}{\mu_F\, p_1}$.
The estimate P_0 tells us how often we can perform the forecast based on this pattern. The estimate P_1 tells us how reliable this forecast will be, and the estimate P_2 tells us what fraction of all p_1 in the signal is predictable via the pattern. For example, it may happen that p_0 is always followed by p_1 which makes this combination of patterns a reliable prediction ($P_1 = 1$). If in the same time, p_1 is preceded by many other patterns, then $(p_0 \times p_1)$ is reliable but not very efficient combination ($P_2 \approx 0$). Finally, if besides the above-stated, p_0 alone is not frequently observed then the prediction is reliable but practically useless, as one has to wait long, before the opportunity to assert a forecast comes ($P_0 \approx 0$). And so the problem of good forecasting given a sample of the signal shapes as a search for such $p \in \mathcal{F}$ that scores high on all three estimates P_0, P_1, P_2. Below, we will consider a few semi-heuristic choices on how such a search can be performed.

5.4.1 Markov model

Let $W_F = \{[b_{i-1}, b_i],\ i = 1, \ldots, n : b_i > b_{i-1},\ b_i \in (0, \infty)\}$, $W_T = (0, \infty)$ and $d = 2$. We search for patterns from $p \in (W_F \times W_T)^d \subset \mathcal{F}$. We are discretising the peak height into n bins and ignore the duration of the peaks completely.

This way, the prediction scheme with $d = 2$ becomes identical to a Markov chain. To do this, we classify the wave heights in a number of bins and then count how often transitions between bins occur. We can also include a finite history, by classifying wave heights of two successive extrema and counting transitions between pairs of extrema or by counting for how many successive extrema the waves are above a certain threshold before a quiescent period is entered. An optimised combination of bin widths, number of bins and history depth will be needed for the best possible prediction, but a full exploration of all these algorithmic choices is beyond our scope here.

We consider the wave heights for a run of 5 hours. In these 5 hours there are 5212 extrema in the data, with the largest deviation from the mean equal to 1.47 meters.

Bin	0-0.198	0.198-0.323	0.323-0.448	0.448-0.607	0.607-1.47
Number of extrema	1041	1042	1043	1042	1043

Table 3: Numbers of peaks in each bin from the chosen system of 5 bins

We choose to use 5 bins, with the limits on the bins such that each of the 5 intervals specified by the bins has equal numbers of extrema. This is summarised in table 3. The slight variation in numbers of extrema is due to rounding on the bin widths. We now simply count the transitions between bins and use this to construct a matrix $\hat{M}_2$ that, at index (n, m), counts how often a wave of height n evolves into height m:

$$\hat{M}_2 = \begin{pmatrix} 620 & 294 & 104 & 24 & 0 \\ 291 & 353 & 252 & 122 & 24 \\ 99 & 266 & 344 & 261 & 73 \\ 26 & 105 & 273 & 399 & 238 \\ 5 & 24 & 70 & 236 & 708 \end{pmatrix}. \tag{49}$$

It is clear that there is some structure in the wave pattern, namely that waves of a certain height are likely to be followed by waves of comparable height.

The question whether it is sufficient to only consider a history depth of one extremum may be raised. This assumption underlying the analysis leading to $\hat{M}_2$ may simply be tested using the data. To do this we first normalise the columns of $\hat{M}_2$ to 1, which makes it into a probability transition matrix M_2. The normalisation is chosen such that if we are in a state and multiply it from the left with M_2, we always go to some other state and the total probability of being in any state is conserved. We can then compute M_2^2, which models the process of taking two steps with our Markov model M_2, and compare it to the transition matrix that skips over one extremum, M_2^s. Then, if the assumption that only the current state matters for forecasting holds, we should have that $M_2^2 = M_2^s$. These two matrices are shown in below:

$$M_2^2 = \begin{pmatrix} 0.44 & 0.29 & 0.17 & 0.08 & 0.02 \\ 0.29 & 0.27 & 0.22 & 0.16 & 0.07 \\ 0.17 & 0.22 & 0.25 & 0.23 & 0.13 \\ 0.08 & 0.15 & 0.23 & 0.28 & 0.26 \\ 0.02 & 0.06 & 0.13 & 0.26 & 0.52 \end{pmatrix}, \quad M_2^s = \begin{pmatrix} 0.31 & 0.29 & 0.22 & 0.13 & 0.05 \\ 0.30 & 0.25 & 0.18 & 0.17 & 0.11 \\ 0.20 & 0.21 & 0.22 & 0.22 & 0.15 \\ 0.14 & 0.15 & 0.22 & 0.25 & 0.24 \\ 0.05 & 0.10 & 0.16 & 0.23 & 0.46 \end{pmatrix}. \tag{50}$$

It can be seen from Eq. (50) that M_2^2 and M_2^s are not identical. The question is then if this is just because we do not have enough data, or because our modelling choice of having the bins in table 3 and considering a state space of only the current extremum is not good enough. To test this properly, we need a way of comparing these matrices while taking into account that due to statistical fluctuations we expect the estimation of transition probabilities of rare events to be worse than the estimation for common events. Furthermore, we would like to be able to compare matrices of different sizes, because changing the number of bins or history depth changes the size of the state space and hence the dimensions of the matrices. Let $n = 5212$ be the

number of extrema, $\hat{M}_2^s$ the unnormalised version of M_2^s, $\times$ the element-wise product of matrices, and $||.||_F$ the Frobenius norm and define

$$e(\hat{M}^s, M^s, M, n) := ||\hat{M}^s \times (M^s - M) \times (M^s - M)||_F/n. \tag{51}$$

Then $e(\hat{M}_2^s, M_2^s, M_2, 5212) = 0.0021$. To interpret this number we shall compare it to the Markov model for the state space with the same bins, but with a history of two extrema. The corresponding 25×25 transition probability matrices are not shown here, but inspection of their entries shows that after a sharp decline in extremum height the likelihood of multiple low extrema is highest. The estimation quality is given by $e(\hat{M}_4^s, M_4^s, M_4, 5212) = 0.00046$. We conclude that the data are better described by taking a longer history depth and that multiple low extrema are most likely if a sharp decline in extremum height is found.

5.4.2 Counting waves

An obvious way to account for longer history is to simply increase the pattern length d in the previous approach. Such decision will quickly lead us to a big number of patterns each with a very low frequency of occurrence and hence poorly represented in finite samples of the signal. We will instead construct a heuristic system of patterns that covers a big part of the whole configurational space and is a formalization of the already observed strategy described by HLO: counting peaks.

A pattern for a single peak with a height below a quiescent threshold, b_q, is given by

$$p_q = (0, b_q] \times [0, \infty).$$

If a peak belongs to this pattern, its height $F_i \in (0, b_q]$ and the duration is arbitrary $T_i \in (0, \infty)$. In a similar fashion we define a pattern with non-zero number of peaks having all the heights below b_q and the total duration exceeding t_q.

$$p_Q = \bigcup_{k=1}^{\infty} \bigcup_{\sum q_i \geq t_q} \bigotimes_{i=1}^{k} (0, b_q] \times [q_i, \infty).$$

If – on a signal fragment $S - \mu_S\, p_Q > 0$, then $\mu_S\, p_q > 0$. Consider now a sequence of $k+2$ peaks that consists of: a peak below the quiescence threshold b_q, k peaks above the threshold b_s, and again a peak below the threshold b_q. The corresponding pattern is given by

$$p_k = p_q \times ([b_s, \infty) \times (0, \infty))^k \times p_q.$$

Now the idea is to investigate the occurrence of patterns $p_k \times p_Q$ for $k = 1, \ldots$ This idea has a very simple practical interpretation.
Suppose one is counting all peaks above the threshold b_s. Every time a peak with amplitude below $b_q < b_s$ comes, one resets the counter to zero. We would like to know whether the count number at the resetting helps in predicting long quiescent periods.

An example of matching patterns from this system to the data is given in Figure 18. As before, we investigate the efficiency of the forecasting according to three measures:

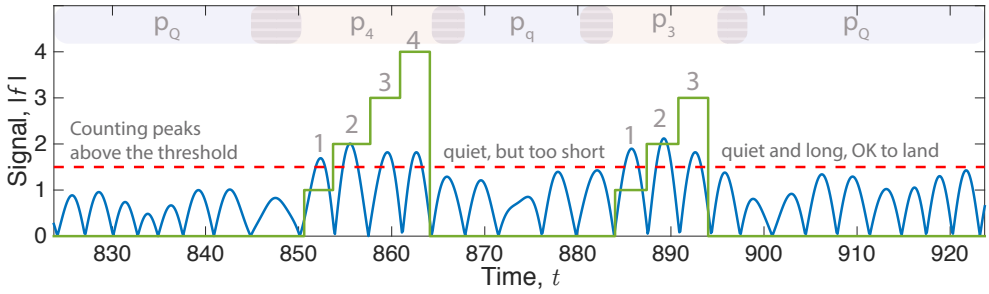

Figure 18: A sample of the signal form dataset D1 together with a matched system of patterns.

P_0, P_1, P_2. Figure 19 presents results for dataset D1 (see Table 2). The figure rates patterns p_k according to measure P_1 (top panel) and T/P_0 (bottom panel), where T is the average distance between peaks. There are a few empirical observations to make here. Firstly, not all patterns are equally good in the prediction. Secondly, the longer a pattern is, the less frequently it is represented in the signal. Thirdly, we see an artefact caused by the finite size of the signal sample: pattern p_9 predicts the quiescence period with probability one precisely because it occurred only once in the sample. On another hand, p_6 leads to very certain predictions, yet its average waiting time, approximately 30 min, is longer then practical limitations. In principle, one can combine p_6 with a pattern that occurs more frequently but has a lower prediction rate, say p_1, to compromise on predictability and reduce the waiting time. Additionally, the partition into patterns is based on parameters b_q, b_s, t_q. While b_q and t_q define the quiescent period and cannot be adjusted, b_s is a free parameter that may influence the quality of the predictions. This motivates the following optimization procedure. Let $\omega_k = \frac{P_0(p_k)}{\sum_{k=1}^{\infty} P_0(p_k)}$ are relative frequencies for pattern k, then the cost function

$$c(k_1, k_2, \dots) = \frac{\sum_{i=1}^{\infty} \omega_{k_i} P_1(P_{k_i})}{\sum_{i=1}^{\infty} \omega_{k_i}}$$

gives the average prediction rate for a union of patterns p_{k_i}, where k_i form a subset in $\mathbb{N}$. The task is to choose such a subset of indexes that the union of the corresponding patterns has best expected prediction rate. This requirements are crystallized as the

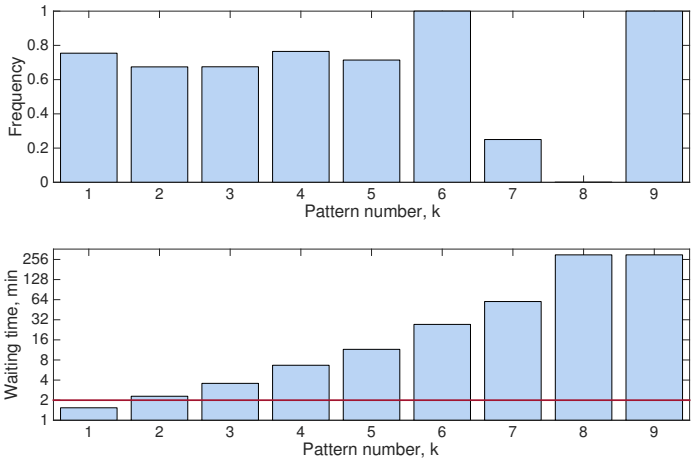

Figure 19: Efficiency of forecasts due to patterns p_k, as measured according to forecast certainty P_1 and waiting the time $1/P_0$. The values for method parameters are: $b_s = 1.72$.

following optimization problem,

$$\begin{aligned} c(k_1, k_2, \dots) &\to \min, \\ \{k_1, k_2 \dots\} &\subset \mathbb{N}, \\ \mathrm{w}_t\left(\bigotimes_i p_{k_i}\right) &\leq w_{\max} \\ b_s &\in [b_q, \infty), \end{aligned}$$

where $\mathrm{w}_t(p)$ denotes the waiting time for a pattern p, and $w_{\max}$ is the upper constrain on the waiting time, in this report $w_{\max} = 2$ min unless stated otherwise.

Figure 20 features the prediction rates and waiting times for patterns after such an optimisation has been carried out for dataset D1 (see Table 2). The resulting optimal subset of indexes is $S_o = \{1, 2, 4, 5, 6, 7, 9, 10\}$ and the optimal value for $b_s = 1.5750$. The optimal set of parameters leads to the expected prediction rate 0.74; the occurrences of the combined prediction pattern $\bigotimes_{k \in S_o} p_k$ are separated by average waiting time of 1.85 min. In total, 78% of all quiescent periods are predictable via this combined pattern. This frequency of predictable events is limited by two factors: the choice for the pattern, which is in part heuristic and thus can be improved; the randomness of the signal that is a feature of data and cannot be manipulated.

All in all, we performed prediction tests/optimisation of the patterns on four datasets, shortly referred to as D1, D2, D3, D4, as shown in Table 2.

Table 4 provides the quality measures for all combination of optimisation/prediction. Data sets D1, D2 are two finite uncorrected samples produced for the same model

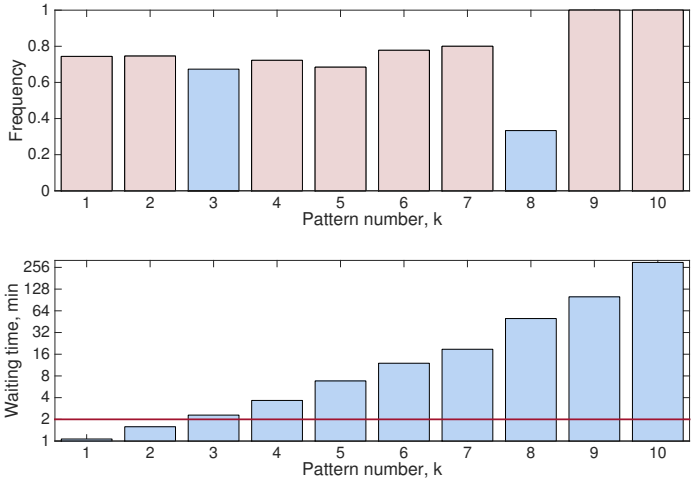

Figure 20: Efficiency of forecasts due to patterns p_k, as measured according to forecast certainty P_1 and waiting the time $1/P_0$. The values for method parameters are: $b_s = 1.545$.

Opt. \ Test	D1	D2	D3	D4
D1	$\chi = 0.804$ $t = 1.33$ $f = 0.30$	$\chi = 0.68$ $t = 2.0$ $f = 0.79$	$\chi = 0.53$ $t = 3.0$ $f = 0.55$	$\chi = 0.12$ $t = 5.0$ $f = 0.75$
D2	$\chi = 0.73$ $t = 1.73$ $f = 0.83$	$\chi = 0.71$ $t = 1.87$ $f = 0.87$	$\chi = 0.58$ $t = 2.30$ $f = 0.72$	$\chi = 0.12$ $t = 7.5$ $f = 0.5$
D3	$\chi = 0.74$ $t = 2.0$ $f = 0.7$	$\chi = 0.71$ $t = 2.10$ $f = 0.78$	$\chi = 0.74$ $t = 1.87$ $f = 0.89$	$\chi = 0.09$ $t = 10$ $f = 0.37$
D4*	$\chi = 0.76$ $t = 17.60$ $f = 0.08$	$\chi = 0.76$ $t = 15.0$ $f = 0.1$	$\chi = 0$ $t = \mathrm{n/a}$ $f = 0$	$\chi = 0.67$ $t = 7.5$ $f = 0.5$

Table 4: Prediction and pattern optimisation on various datasets. The prediction quality is measured by certainty χ, pattern waiting time t (min) and fraction of predictable events, f. *For optimisation on dataset D4 the upper constrain on average waiting time was relaxed to $w_{\max} = 8$ min.

parameters. One notices that the prediction quality changes little if we optimise on D1 and then predict on D2 or D3 as opposed to the scenario when we optimise and predict on the same dataset. This may suggest that the optimised pattern grasps some universal property of the data. The situation changes when we analyse datasets with distinct simulation parameters, e.g. comparing dataset D1 to D4, that features larger wave height. In this case, when trained on D1, the prediction certainty on D4 is much smaller. When trained on D4 and then predicting on D1 the prediction certainty is relatively high but the waiting time is a magnitude larger. This scenario demonstrates that the optimised pattern does depend on the software parameters (that, in turn, mimic the sea state).

Optimisation on D4 results in no solution unless we increase the upper constraint on the waiting time. Such behaviour is connected to the fact that there are not many quiescent periods in this dataset.

5.5 Summary

Instead of processing the full data from the motion sensor, we narrowed our attention to the sequence of extrema values (the peaks). Patterns in such a sequence are defined as a subsequence of peaks with heights that fall within specific bounds. From this point of view a pattern is a manifold in the the peak configuration space. Given an observed sequence, the frequency of pattern occurrence can be computed as number of times such manifold was hit by samples form the data. Special interest present those patterns that combine non-quiescent period followed by a quiescent one.

Software-simulated data were analyzed for occurrence of patterns. Similar patterns were found in uncorrelated sample data that were produced with the same simulation parameters specifying the sea state. The patterns differ when different sea-state parameters are used. A somewhat naive choice for patterns as a tensor product allows one to assert predictions on quiescent period with 80% certainty and acceptable (from operation time point of view) frequency on some datasets. We expect that the certainty can be improved by a cleverer choice for pattern manifolds.

6 Conclusions

Given several simulations of ship motion, we tried to identify the distribution and initiation of quiescent periods (QPs) by various techniques with the common aim of pattern recognition. Moreover, within reasonable assumptions on the response of the ship to the forcing of the sea waves, we claimed that studying the more general problem of finding QPs in a sum of random harmonic is relevant to make statements about the occurrence of QPs in ship motion.

The first thing we realized is that the essential information of the motion is contained in the extrema of the waves, and that this is encoded in the Hilbert transform of the signal. We then gave a statistical description of the distribution of QPs and a qualitative picture of the typical ship motion around a QP. While the former suggests

modeling the occurrence of QPs by a Poisson process (even though this argument has still to be statistically tested), the latter information constitutes the first tool that we have for prediction of QPs.

Whenever ship motion is essentially coincident with the sea motion and its spectrum is narrow-banded, we gave analytical estimates of both probability and frequency of quiescent periods in a sum of deterministic and random harmonics. We reviewed the cases of one, two and three deterministic harmonics: the second one encodes the phenomenon of beating and is the prototype to have a first understanding and definition of a quiescent period; the third case already contains a lot of the features of the most general case.

We then considered the case of arbitrarily many random harmonics. First, we applied existing methods to characterize rates of upcrossing of a fixed threshold. Next, we gave estimates for the distribution of QPs according to two different definitions of a QP and in terms of both the hight and the length of a QP.

The methods of fast prediction of quiescent periods are based on recognizing pattern in the time series via Fourier continuation and a few stochastic models for stationary processes. While the former, at this level of analysis, doesn't seem to be useful, the latter look promising. Indeed, we were able to identify several structural properties in the data.

The methods via the extrapolation problem perform well in the case of short-term prediction, but deteriorate when prediction is sought for longer futures. The autoregressive models are able to provide a reasonable forecast in some cases, but with rather scarce statistical confidence. A logistic regression was proposed, too, but it has still to be tested, together with a change-point-detection procedure. We remark that the simulations we have performed are limited to the data series of the heave coordinate. We feel that the inclusion of other variables may help the predictive power of such models.

The final approach described in this report is looking at the data from the standpoint of the theory of Markov processes. We were able to identify a few waves patterns, interpret the data as a random sequence of patterns, investigate the "memory content" of that stochastic process, and implement prediction. Some patterns gave rise to fairly good predictions, specifically when a series of particularly high waves are followed by a QP. We expect that this could be improved further by a better choice of the patterns themselves.

We are very thankful to MARIN, in particular in the persons of Ed van Daalen and Jos Koning for giving us such a interesting and stimulating challenge. We hope that this work will give MARIN sufficient motivation and inspiration to continue the project with new ideas and renovated enthusiasm.

References

M. Basseville and I. V. Nikiforov. *Detection of Abrupt Changes: Theory and Application.* Englewood Cliffs, Prentice Hall, N. J., 1993.

P. Bloomfield. *Fourier analysis of time series: An introduction*. Hoboken, John Wiley & Sons, 2000.

P. J. Brockwell and R. A. Davis. *Time series: theory and methods*. Springer Series in Statistics. Springer-Verlag New York, 2009.

CalQlata. *RAO Calculator*. URL `http://www.calqlata.com/productpages/00081-help.html`. [accessed on 31-03-2017].

J. Chen and A. Gupta. *Parametric Statistical Change Point Analysis: with Applications to Genetics, Medicine, and Finance*. Springer-Verlag Berlin, 2012.

H. Cramér and M. Leadbetter. *Stationary and related stochastic processes: Sample function properties and their applications*. Mineola, Dover Publications, 1967.

B. Fristedt, N. Jain, and N. Krylov. *Filtering and prediction: a primer*. Providence, American Mathematical Society, 2007.

G. Hardy and E. Wright. *An introduction to the theory of numbers*. Oxford University Press, fifth edition edition, 1979.

R. Kabacoff. *R in Action: Data Analysis and Graphics with R*. Manning Publications Co., Greenwich, CT, USA, 2015. ISBN 1617291382, 9781617291388.

J. Kuhn, W. Ellens, and M. Mandjes. Detecting changes in the scale of dependent Gaussian processes: A large deviations approach. In B. Sericola, M. Telek, and G. Horváth, editors, *Analytical and Stochastic Modeling Techniques and Applications*, Lecture Notes in Computer Science, pages 170–184. Springer International Publishing, 2014.

J. Kuhn, M. Mandjes, and T. Taimre. False alarm control for change point detection: Beyond ARL. *Submitted*, 2016.

G. Lindgren. *Stationary stochastic processes: Theory and applications*. Boca Raton, CRC Press, 2013.

MARIN. *Dynamic Stability Simulation*. URL `http://www.marin.nl/web/Facilities-Tools/Software/Dynamic-Stability-Simulation.htm`. [accessed on 31-03-2017].

L. Nirenberg. On elliptic partial differential equations. In *Il principio di minimo e sue applicazioni alle equazioni funzionali*, pages 1–48. Springer, 2011.

E. Page. Continuous inspection scheme. *Biometrika*, 41:100–115, 1954.

S. Rice. Mathematical analysis of random noise. *Bell System Technical Journal*, 23: 282–332, 1944.

M. Robbins, C. Gallagher, R. Lund, and A. Aue. Mean shift testing in correlated data. *Journal of Time Series Analysis*, 32:498–511, 2011.